The OLYMPUS Experiment

R. Alarcon, L.D. Ice

Arizona State University, Tempe, AZ, USA

F. Brinker, N. D'Ascenzo, N. Goerrissen, J. Hauschildt, Y. Holler, D. Lenz, U. Schneekloth

Deutsches Elektronen-Synchrotron, Hamburg, Germany

D. Bayadilov, R. Beck, D. Eversheim, Ch. Funke, Ph. Hoffmeister, P. Klassen, A. Thiel

Rheinische Friedrich Wilhelms Universität Bonn, Bonn, Germany

O. Ates, J. Diefenbach, M. Kohl

Hampton University, Hampton, VA, USA

R. De Leo, R. Perrino

Istituto Nazionale di Fisica Nucleare, Bari, Italy

V. Carassiti, G. Ciullo, M. Contalbrigo, P. Lenisa, M. Statera

Universita' di Ferrara and Istituto Nazionale di Fisica Nucleare, Ferrara, Italy

E. Cisbani, S. Frullani

Istituto Nazionale di Fisica Nucleare, Rome, Italy

B. Glaeser, D. Khaneft, Y. Ma, F. Maas, R. Pérez Benito, D. Rodríguez Piñeiro

Johannes Gutenberg Universität, Mainz, Germany

J.C. Bernauer, J. Bessuille, B. Buck, T.W. Donnelly, K. Dow, D.K. Hasell*, B. Henderson, J. Kelsey, R. Milner, C. O'Connor, R.P. Redwine, R. Russell, A. Schmidt, C. Vidal, A. Winnebeck

*Corresponding Author

Email address: hasell@mit.edu (D.K. Hasell)

[1]Also with Universita' di Ferrara and Istituto Nazionale di Fisica Nucleare, Ferrara, Italy

Preprint submitted to Nuclear Instruments and Methods A *October 4, 2013*

Massachusetts Institute of Technology, Cambridge, MA, USA

V.A. Andreev, S. Belostoski, G. Gavrilov, A. Izotov, A. Kiselev, A. Krivshich, O. Miklukho, Y. Naryshkin, D. Veretennikov

Petersburg Nuclear Physics Institute, Gatchina, Russia

R. Kaiser, I. Lehmann, S. Lumsden, M. Murray, G. Rosner, B. Seitz

University of Glasgow, Glasgow, United Kingdom

J.R. Calarco

University of New Hampshire, Durham, NH, USA

N. Akopov, A. Avetisyan, G. Elbakian, G. Karyan, H. Marukyan, A. Movsisyan[1], H. Vardanyan, V. Yeganov

Yerevan Physics Institute, Yerevan, Armenia

Abstract

The OLYMPUS experiment was designed to measure the two-photon contribution in elastic electron-proton scattering. Two-photon exchange could explain the discrepancy between measurements of the form factor ratio, $\mu_p G_E^p / G_M^p$, made using polarization techniques and those made in unpolarized experiments. To achieve its goal, OLYMPUS operated on the DORIS storage ring at DESY with electron and positron beams at 2.01 GeV incident on an internal hydrogen gas target to determine the ratio of elastic scattering cross sections for positrons versus electrons. The experiment used a toroidal magnetic spectrometer instrumented with drift chambers and time of flight detectors to measure rates for elastic scattering over the polar angular range of approximately 25°–75°. A symmetric Møller / Bhabha calorimeter at 1.29° and telescopes of GEM and MWPC detectors at 12° served as luminosity monitors. A total luminosity of ~ 4.4 fb^{-1} was collected. This paper provides details on the accelerator, target, detectors, and operation of the experiment.

Keywords: elastic electron scattering, elastic positron scattering, two-photon exchange, form-factor ratio

2010 MSC: 25.30.Bf, 25.30.Hm, 13.60.Fz, 13.40.Gp, 29.30.-h

1. Introduction

The structure of nucleons has long been studied using electromagnetic probes. Point-like electrons and positrons are ideal for this since the lepton vertex is well described by quantum electro-dynamics. The mediating photon (or weak boson at higher energies) can be used to "see" deeper and deeper into the nucleon. As the momentum transfer increases, the measurements progress from the nucleon size to the elastic form factors, G_E and G_M, arising from the distribution of charge and magnetism inside the nucleon. At still higher momentum transfers, deep inelastic scattering reveals the distributions of the quarks and gluons that ultimately must produce the observed form factors and nucleon sizes. The resulting data can then be used to verify our theoretical understanding of the innermost workings of the nucleon. With polarized beams and targets, even more details are available.

Recently, measurements of the electric to magnetic form factor ratio, $\mu_p G_E^p / G_M^p$, using polarization techniques (1–8) have shown a dramatic discrepancy in comparison with the ratio obtained using the traditional Rosenbluth technique in unpolarized cross section measurements (9–12) as shown in Fig. 1. This discrepancy may be explained as arising from multiple-photon exchange beyond the usual one-photon exchange. Since most of our understanding on the structure of the proton has assumed a single mediating photon, it is essential to quantify the contribution of multiple-photon exchange and whether this explains the discrepancy or if there is some other contributing process.

To address this question, the OLYMPUS experiment was proposed to measure the ratio between the positron-proton and electron-proton elastic scattering cross sections. This ratio would be unity if only single photon exchange occurred. However, if multiple-photon exchange contributes significantly, the ratio will deviate from unity because the interference term between single- and double-photon exchange will change sign between electron and positron scattering. This ratio was measured in the 1960s with some indication of a deviation from unity but the uncertainties were large. This is shown in Fig. 2 together with some theoretical calculations and the projected OLYMPUS data.

The OLYMPUS experiment was approved for three months of dedicated operation on the DORIS electron/positron storage ring at the DESY laboratory in Hamburg, Germany. An unpolarized, hydrogen gas target was designed and built at MIT to be installed internally on the DORIS ring. To

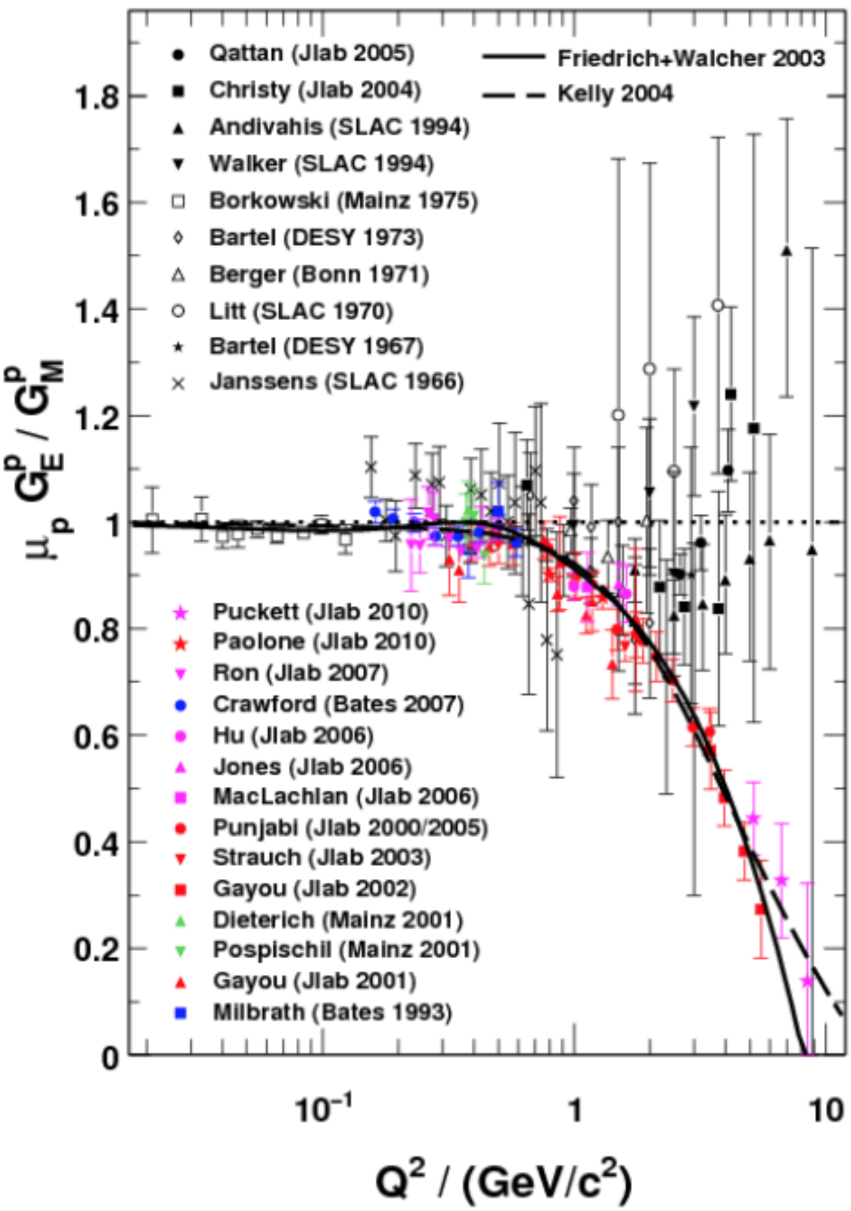

Fig. 1: Ratio of proton form factors $\mu_p G_E^p / G_M^p$ as a function of Q^2 showing results from unpolarized measurements in black and recent data measured using polarized techniques.

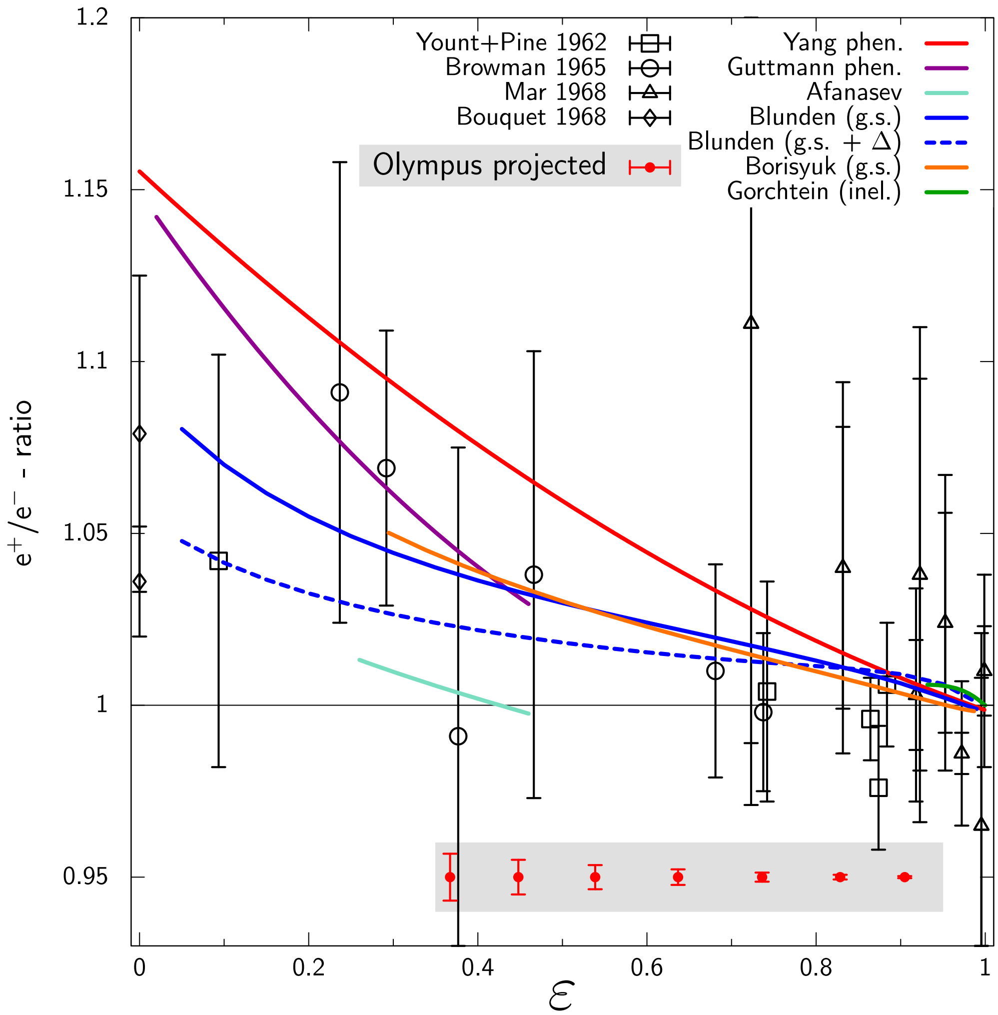

Fig. 2: Ratio of positron to electron elastic scattering cross section as a function of ϵ showing existing data, some theoretical predictions, and projected OLYMPUS data range and uncertainties.

measure the ratio in elastic scattering cross sections, the former BLAST detector was shipped from MIT-Bates to DESY and installed on the DORIS ring. The detector used a toroidal magnetic field with a left/right symmetric arrangement of tracking detectors and time of flight scintillators. In addition, three new detector systems were designed and built to monitor the luminosity during the experiment. These were a symmetric Møller/Bhabha calorimeter from Mainz at 1.29° and telescopes of triple GEM detectors from Hampton and MWPC detectors from PNPI mounted at 12°. The Bonn group provided the software and hardware for the data acquisition system. The trigger and slow control systems were developed by MIT.

The OLYMPUS experiment collected data in two periods: the February period (January 20 - February 27, 2012) and the Fall period (October 24, 2012 - January 2, 2013). During the February period the beam species was typically changed daily and the magnet polarity was changed randomly, but equally, every 6 hours. For the February data run there was a leak in the target gas supply such that only a fraction of the measured flow reached the target cell. Because of this a lower than expected luminosity was obtained. The gas leak was repaired in the summer so that it was possible to achieve high luminosity in the Fall period. However, it was discovered that at high luminosity and negative magnet polarity too many electrons were bent into the wire chambers preventing their operation. After several tests and attempts to remedy this it was decided to operate at high luminosity but primarily with positive magnet polarity for most of the Fall period.

The following sections describe the accelerator, target, detectors, data acquisition, and operation in more detail.

2. DORIS Storage Ring at DESY

The DORIS storage ring at DESY was originally began operation in 1974 as an electron-electron and electron-positron collider. After its long and successful operation for particle physics research DORIS, was dedicated to synchrotron radiation studies in 1993. Since DORIS had access to both a positron and electron source and could circulate both species at ∼GeV energies, it was a natural candidate for the OLYMPUS experiment. Additionally, the infrastructure at the location in the beamline of the former Argus Experiment (13) provided an excellent match to the size and needs of OLYMPUS. In 2009, the shutdown of DORIS was scheduled for the end of 2012, placing a tight time constraint on OLYMPUS.

Although the DORIS accelerator and the ARGUS detector site were well suited to the OLYMPUS Experiment, several modifications were required. In particular, a number of considerations were necessary to allow DORIS to continue to operate as a synchrotron light source after OLYMPUS was installed (although not during OLYMPUS data taking). These included:

- RF cavities that had been installed at the detector site had to be relocated 26 m upstream.
- An additional quadrupole was installed on each side (±7 m) of the OLYMPUS interaction region to reduce the beam size for the OLYMPUS target while not significantly affecting the beam profile in synchrotron radiation source elements. This was necessary due to the impracticality of removing the OLYMPUS target for synchrotron runs.
- The OLYMPUS target required cooling during synchrotron radiation runs due to the wakefield heating caused by the 150 mA, 4.5 GeV, 5-bunch beam.
- A number of tests and improvements were required to achieve the 10-bunch, 2.01 GeV beam conditions for OLYMPUS operation with adequate currents and lifetimes, including the implementation of a multi-bunch feedback system.

A key feature of the OLYMPUS experiment was the frequent switching between e^- and e^+ beams. The DORIS pre-accelerators were already able to switch between electrons and positrons within $\sim$ 10 minutes, but the extraction from the pre-accelerators to DORIS, the transport line, and the DORIS ring needed several modifications:

- The high voltage pulse power supplies for the pre-accelerator extraction and the DORIS injection kickers had to be rebuilt.

- The septa magnets for pre-accelerator extraction and DORIS injection were modified to serve as bipolar devices.

- Remotely-controlled polarity switchers for a number of 800 A magnet power supplies had to be constructed and installed

The daily switching of the beam species for OLYMPUS posed a challenge for the parallel operation of DORIS and the PETRA storage ring, which shared the same pre-accelerators. While PETRA did not operate during the February run, the procedure for switching the polarity of the pre-accelerators was optimized to accommodate parallel operation during the Fall run. With these improvements, PETRA could be refilled in approximately 5 minutes, causing only a small delay for DORIS refills.

Since the injection into DORIS occurred at full energy, it was possible to run in top-up mode to achieve higher average current, and hence more luminosity. The injection process was optimized to minimize beam losses, which prevented excessive rates in the OLYMPUS detector (which would cause high voltage trips).

The presence of the OLYMPUS gas target increased the radiation levels in the region downstream of the experiment relative to synchrotron radiation operation. Additional shielding was installed to account for this. Also, the beam scrapers upstream of the experiment were optimized to minimize the noise rates in the experiment.

To monitor the beam energy, a dipole reference magnet was installed in series with the DORIS dipole magnets. This magnet included a rotating coil to measure the integrated field strength. The accelerator archive system monitored all relevant data, power supply currents for all magnets, beam position data, scraper positions, etc. and provided much of this information to the OLYMPUS slow control system.

3. Target and Vacuum Systems

The OLYMPUS experiment used an unpolarized, internal hydrogen gas target cooled to below 70 K. The hydrogen gas flowed into an open-ended, 600 mm long, elliptical target cell (Sec. 3.1). The target cell was housed in a scattering chamber (Sec. 3.2) that had thin windows to match the angular acceptance of the detectors. A tungsten collimator (Sec. 3.4) was also housed in the scattering chamber to prevent synchrotron radiation, beam halo, and off-momentum particles from striking the target cell. Additionally, a series of wakefield suppressors (Sec. 3.3) were necessary to reduce the heat load on the target cell. Finally, an extensive vacuum system (Sec. 3.5) of turbomolecular and Non-Evaporable Getter (NEG) pumps was employed to preserve the vacuum in the DORIS storage ring.

3.1. Target Cell

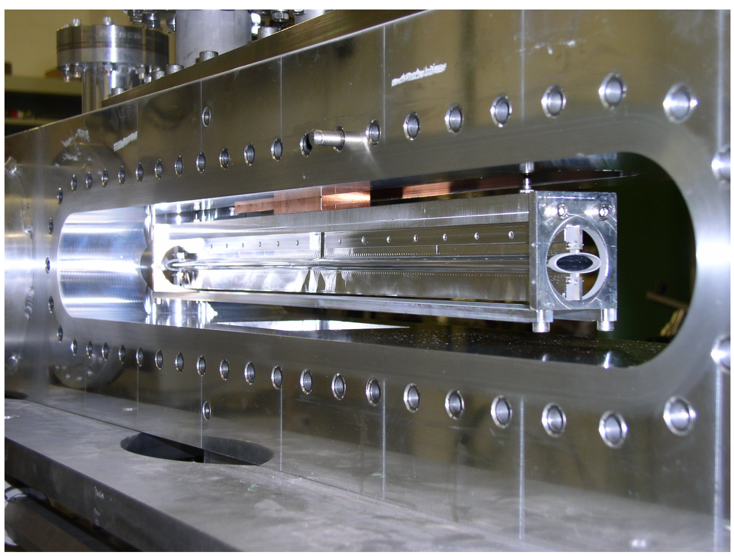

Fig. 3: Photograph of one of the OLYMPUS target cells mounted inside the scattering chamber.

The target cell consisted of an open-ended, elliptical cylinder (27 mm horizontal$\times$9 mm vertical$\times$600 mm long) made from 0.075 mm thick aluminum. The elliptical shape was chosen to match the DORIS beam envelope and was set to approximately the 10σ nominal horizontal and vertical beam width at the OLYMPUS interaction point to minimize the amount of beam halo striking the cell walls.

Several cells were fabricated over the course of the experiment at INFN, Ferrara. Cells were formed from two identical stamped sheets of aluminum that were spot welded together along the top and bottom seams. Each cell was mounted in a frame by a clamp that ran the entire length of the top seam. The frame was made of 6063 aluminum to provide high themal conductivity at cryogenic temperatures. When installed in the scattering chamber, the cell and frame assembly was suspended from a flange in the top of the scattering chamber (shown in Fig. 3) and its position and orientation could be adjusted. The entire cell and frame assembly were cooled by a cryogenic coldhead. The assembly was wrapped in several layers of aluminized mylar to insulate it from thermal radiation. Without beam, or gas flow, the target could reach temperatures below 40 K. During high luminosity running, a temperature of about 70 K was sustained.

During operation, hydrogen gas was flowed through the target cell. The hyrogen gas was produced by a commerical hydrogen generator and was controlled by a series of valves, buffer volumes, and mass flow controllers. The gas entered the cell at the center, from a tube that fit snuggly into an opening of the cell's top seam. The gas diffused outwards to the open ends of the cell, where it was removed by the vacuum system. This diffusion was slowed because the hydrogen quickly cooled to the temperature of the cell. The density distribution in the cell was triangular, with peak density at the center of the cell falling to zero density at either end. A flow rate of 1.5×10^{17} H_2 atoms per second was required to produce a target thickness of 3×10^{15} atoms cm^{-2}.

3.2. Scattering Chamber

The OLYMPUS scattering chamber (shown in Fig. 4) was 1.2 m long and was machined from a solid block of aluminum, with large area windows on the left and right faces. The windows were made of 0.25 mm thick 1100 aluminum, and nominally subtended a polar angular range of 8° to 100° from the center of the target, 6° to 90° from 200 mm upstream, and 10° to 120° from 200 mm downstream. The chamber was trapezoidal in shape to angle the windows forward to make more of the target cell "visible" to the 12° detectors.

In addition to windows, the chamber had ports for the beamline (up- and downstream), for pumping (on the bottom surface), and for access to

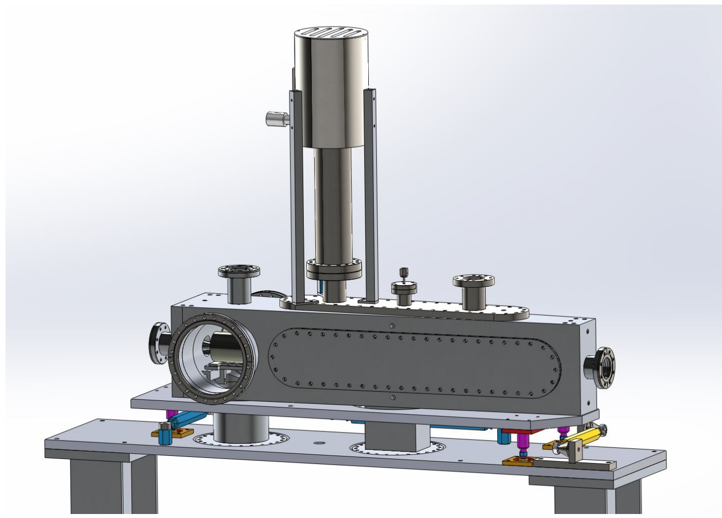

Fig. 4: CAD model of the OLYMPUS scattering chamber.

the collimator (on the left and right), as well as the target cell flange on the top, which had feedthroughs for the hydrogen gas, the coldhead, and various sensors. The main components inside the scattering chamber are shown in Fig. 5.

3.3. Wakefield Suppressors

Wakefield suppressors were necessary to maintain the target cell at cryogenic temperatures by preventing heating caused by wakefields. The wakefield supressors consisted of conducting transitions that were added to fill gaps between conducting structures surrounding the beam. Any sharp transitions or gaps in conductivity would serve as electrical cavities that would be excited by the passing beam, creating wakefields and producing heat. To prevent this, three wakefield suppressors were produced to cover the following transitions:

1. from the circular upstream scattering chamber port (60 mm in diameter) to the 25 mm by 7 mm elliptical opening of the collimator,
2. from the exit of the collimator to the entrance of the target cell (both 27 mm by 9 mm ellipses), and
3. from the 27 mm by 9 mm elliptical exit of the target cell to the circular downstream scattering chamber port (60 mm in diameter).

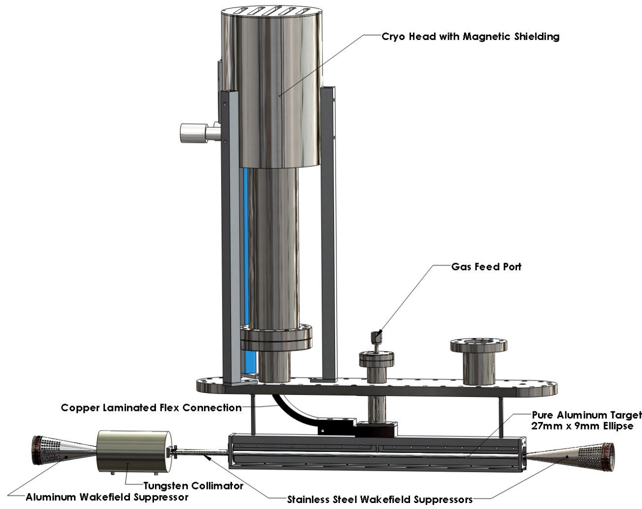

Fig. 5: CAD model of the target cell, wakefield suppressors, and collimator inside the OLYMPUS scattering chamber.

With these wakefield suppressors, a target temperature of around 50 K was maintained during operation with beam.

The wakefield suppressors were made of stainless steel (except the upstream wakefield suppressor, which was made of aluminum), and plated with silver for improved electrical conductivity. The surfaces were smooth except for many small holes, which were drilled to allow the vacuum system to pump gas through them. The ends of the wakefield suppressors had beryllium-copper spring fingers around their circumference. These spring fingers made sliding connections at an interface that allowed for thermal expansion while maintaining good electrical contact. The upstream wakefield suppressor was screwed directly to the collimator, while making a sliding connection with the upstream scattering chamber port. The other two wakefield suppressors were fixed to rings clamped to the ends of the target, and made sliding connections to either the downstream scattering chamber port or the collimator. A close up view of the middle wakefield supressor is shown in Fig. 6).

3.4. Collimator

Fig. 6 also shows the fixed collimator in front of the target cell. The collimator consisted of a 139.7 mm long cylinder of tungsten 82.55 mm in diameter. The outer dimensions were chosen after performing a study on

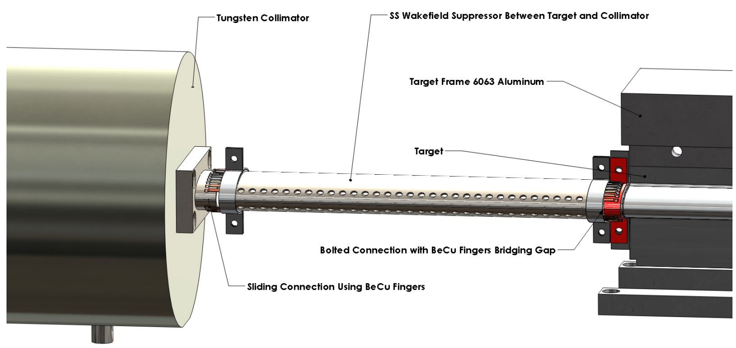

Fig. 6: CAD model of the wakefield suppressor between the collimator and the target cell.

simulated showers of beam-halo particles. It had a tapered elliptical aperture with entrance 25 mm by 7 mm and exit 27 mm by 9 mm. This was machined from a solid block of tungsten using wire electrical discharge machining, EDM[2]. The entrance dimensions were chosen to be slightly smaller than those of the storage cell to shield the target cell walls.

3.5. Vacuum System

A system of magnetic levitation turbomolecular pumps[3] (800 l/s capacity) and NEG pumps[4] (400 l/s capacity) were used to pump the section of beamline inside the OLYMPUS experiment. This consisted of three stages of pumping to reduce the pressure from the relatively high pressure ($\sim 10^{-6}$ Torr) at the scattering chamber (caused by hydrogen gas) to the low pressure ($\sim 10^{-9}$ Torr) of the DORIS storage ring.

The vacuum system is shown in Fig. 7. Six turbomolecular pumps (models Osaka TG 1100M and Edwards STP 1003C) formed a differential pumping system to prevent hydrogen in the target from contaminating the vacuum of the storage ring. Two turbo pumps located in the pit directly beneath the experiment were directly connected to the scattering chamber through 200 mm diameter pipes. Two more turbo pumps were connected to the up- and downstream beamlines approximately 2 m from the target. At approximately 3 m

[2]Jack's Machine Co. Hanson, MA 02341
[3]Osaka and Edwards
[4]SAES Capacitor CFF 4H0402

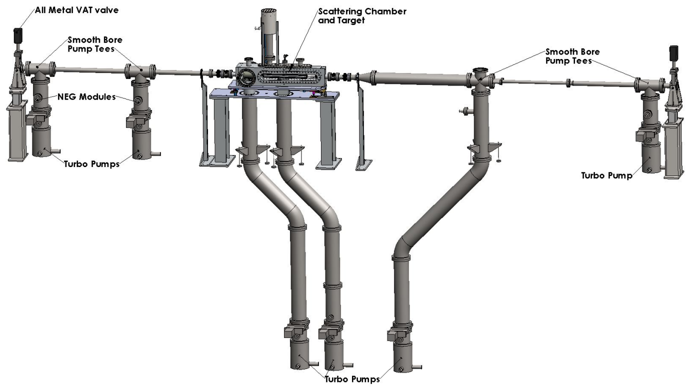

Fig. 7: CAD model of the vacuum system employed on the OLYMPUS experiment.

from the target another two turbo pumps were used to reduce the pressure in the beamline to the level acceptable for the DORIS storage ring. The four pumping stations furthest from the target also had NEG pumps to improve the pumping of hydrogen.

4. The OLYMPUS Detector

The core of the OLYMPUS detector consisted of components from the BLAST spectrometer from MIT-Bates (14). The toroidal magnet, time-of-flight detectors, and many of the readout and control electronics were shipped to DESY in Spring 2010. The components reassembled, reconditioned, and modified as necessary for installation in OLYMPUS detector.

The OLYMPUS Experiment was installed in the straight section of the DORIS storage ring, in the location of the former ARGUS Experiment (13). The site consisted of an approximately 7 m-wide pit extending 5 m beneath the beamline. The pit extended beyond the beamline area into the DORIS hall, with rails above the pit extending its entire length. The OLYMPUS detector was constructed on these rails outside of the DORIS beamline from June 2010 to July 2011, so as to not interfere with DORIS operation. After the completion of the detector construction, the concrete beamline shielding around the experiment site was dismantled, the experiment was rolled-in along the rails, and new shielding was constructed around the detector.

The pit beneath the experiment provided a location sufficiently outside the magnetic field of the detector for the installation of the vacuum pumps, target gas flow system, and low voltage power supplies for the drift chambers. This area, while conveniently near to the detector, was not accessible during DORIS operation.

An electronics "hut" was also supported on the pit rail system and moved with the detector when rolled-in. The beamline shielding was constructed between the hut and the detector (with conduits for cables), to allow access to the hut during operation. The hut housed the detector's readout and control electronics, high voltages supplies, and computer systems. The gas supply systems for the various subdetectors were located outside of the beamline to allow access for gas bottle replacement during operation (or to refill the target system's hydrogen generator with deionized water).

The OLYMPUS spectrometer consisted of an eight-coil toroidal magnet with detector instrumentation in the two sectors of the horizontal plane of the beamline (see Fig. 8). Each of these sectors contained a large drift chamber for particle tracking and and array of time-of-flight scintillator bars for trigger timing and rough energy and particle position measurements. To monitor the luminosity, OLYMPUS had a redundant system of a Symmetric Møller/Bhabha (SYMB) calorimeter at $\theta = 1.29°$ and detector telescopes consisting of three triple gas electron multiplier (GEM) detectors interleaved

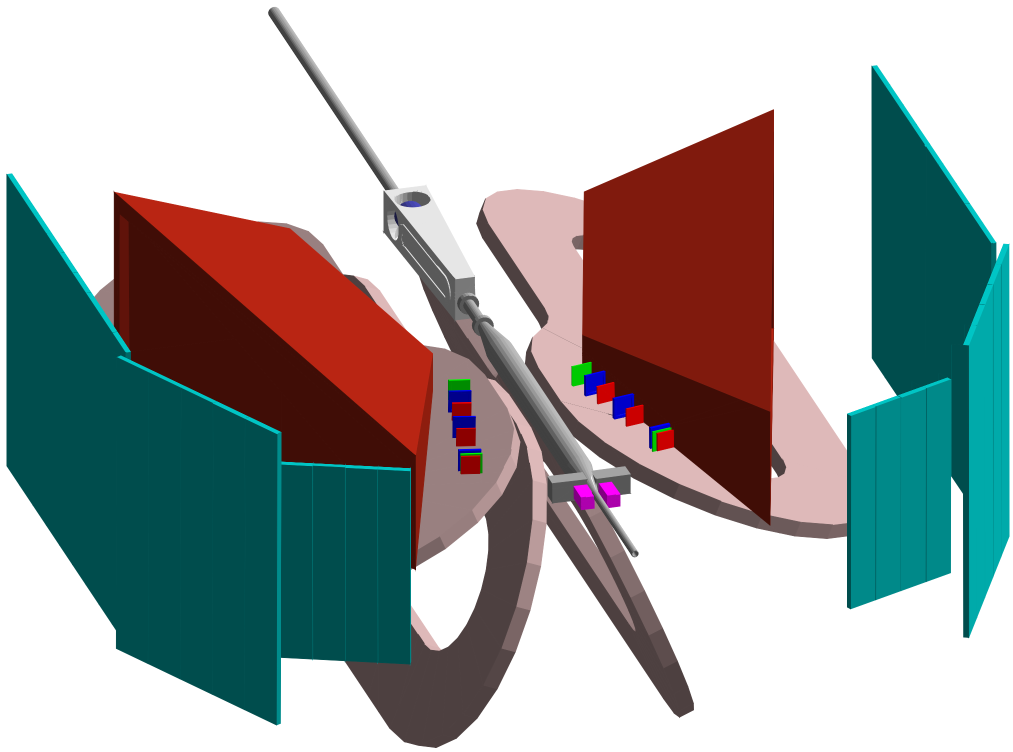

Fig. 8: A solid-model representation of the OLYMPUS detector with the top four magnet coils removed to show the instrumented horizontal sectors.

with three multi-wire proportional chambers (MWPCs) at 12° in both sectors.

The following sections describe the detector components in greater detail.

4.1. Toroidal Magnet

The toroidal magnet consisted of eight copper coils placed around the beam line and scattering chamber so that the beam traveled down the toroid's symmetry axis (see Fig. 9). The coils divided the space around the beamline

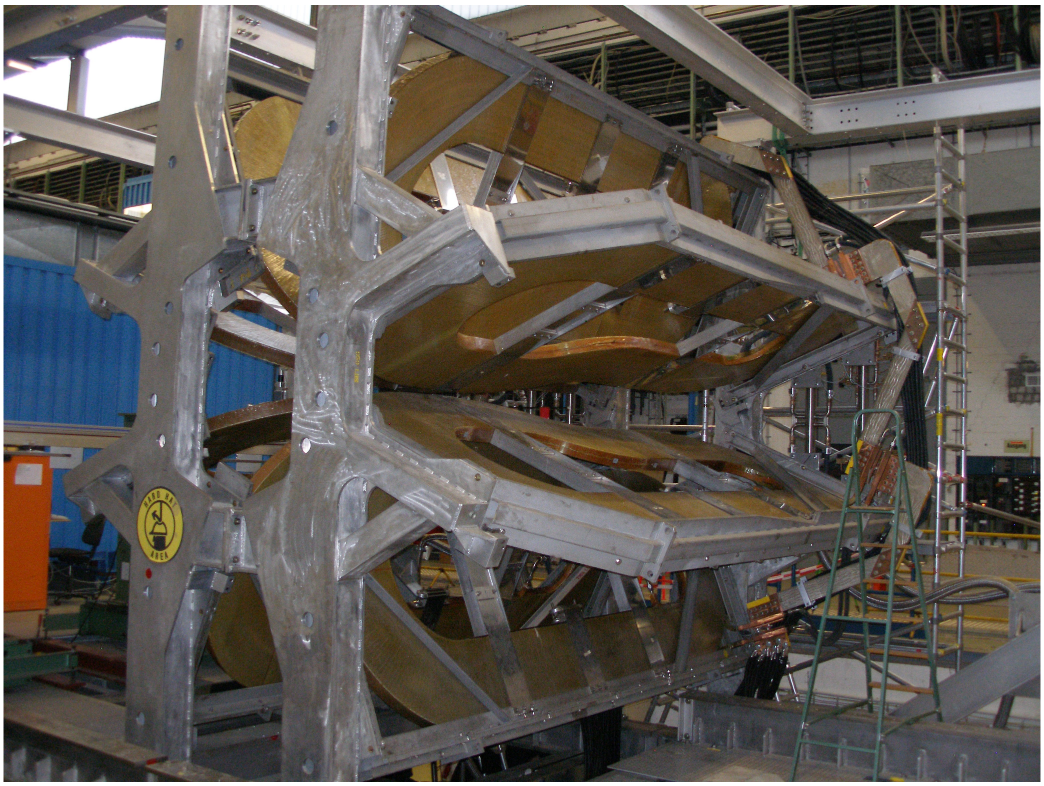

Fig. 9: The toroid magnet assembled at DESY before the subdetectors were installed

into eight sectors. The two sectors in the horizontal plane were instrumented with detectors. During normal operation, the magnet produced a field of about 0.28 T in the region of the tracking detectors.

The magnet was originally designed and used for the BLAST experiment, and has been described in a previous article(15). The choice of a toroidal configuration was made to ensure a small field along the beamline in order to minimize any effects on a spin-polarized beam and to limit field gradients in the region of the polarized target. Since OLYMPUS used neither a polarized beam nor a polarized target, these concerns were not as important. However, during the initial set-up, the magnetic field along the beamline was measured and the coil positions adjusted to achieve an integrated field < 0.005 T·m to avoid perturbing the beam's position or direction.

Each of the toroid's eight coils consisted of 26 turns of 1.5 inch square copper tubes, organized into two layers of 13 turns. A circular hole, 0.8 inches in diameter, ran down the length of each tube and served as a conduit for cooling water. During assembly, the tubes were individually wrapped with fiberglass tape and then collectively potted in an epoxy resin matrix. The final outline and nominal position relative to the beam line and target center at the coordinate origin are shown in Fig. 10. The coils are narrower at one

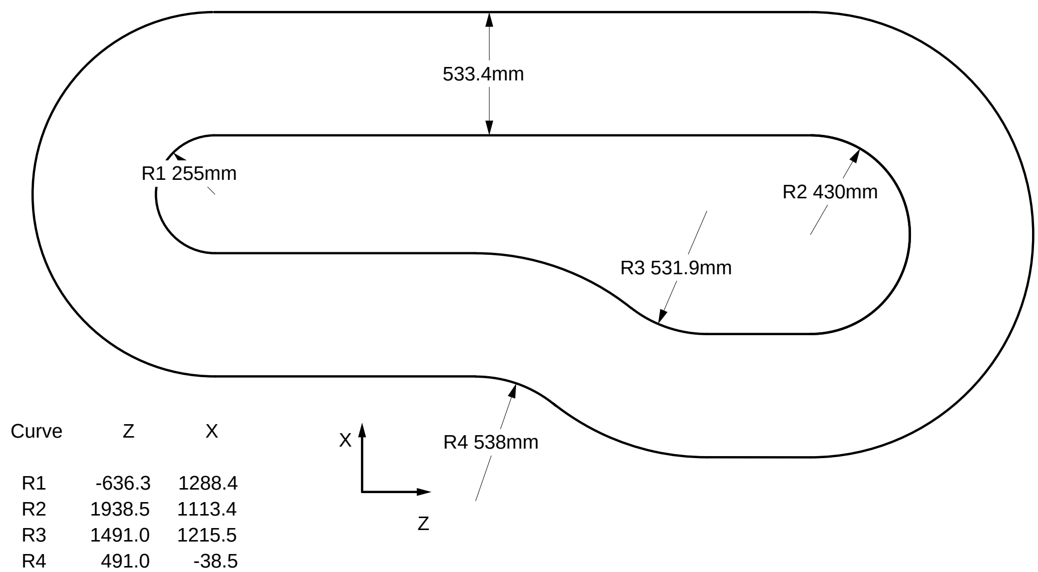

Fig. 10: Plan view of BLAST coil outline showing dimensions and position relative to the center of the target cell.

end to accommodate the scattering chamber and wider at the other to extend the high-field region to more forward angles, where scattered particles have higher momenta.

The magnetic field served two purposes. The first was to bend the tracks of charged particles, allowing their momentum and charge sign to be determined from the curvature of their tracks. The second was to sweep away low-energy, charged background particles from the tracking detectors. Though a stronger magnetic field would have improved momentum resolution and reduced the background, it would also have increased the Lorentz angle of drift electrons in the tracking detectors, making track reconstruction more difficult. A balance was struck by choosing a current of 5000 A for normal operation, which produced a field of about 0.28 T in the high-field regions.

A bipolar 7000 A DC power supply provided current to the toroid. The power supply and the required 10 kV to 480 V transformer were provided by DESY and were installed near the DORIS hall. The supply and the magnet were water-cooled.

Originally, it was planned to alternate the polarity of the magnet every few hours to reduce systematic uncertainties. However, this proved impractical at high-luminosity. In the negative polarity setting, the magnet bent negatively charged particles outward from the beamline. The drift chambers were hit with large background of low-energy electrons, which frequently caused the high-voltage supply to exceed its current threshold and deactivate. Attempts to adequately shield the drift chambers, both by adding material and by increasing the magnetic field strength, were unsuccessful. Consequently, the negative polarity setting was limited to low-luminosity running, and only about 13 % of the total luminosity was collected in this mode. The limited negative polarity data will provide a check on systematic uncertainties.

After the experimental running period was completed, the drift chambers, the 12° luminosity monitors, the Møller detector, and the beamline downstream of the scattering chamber were removed in order to conduct a measurement of the magnetic field. The field region was scanned using a 3D Hall probe mounted to a rod, driven by several translation tables. The rod was mounted to a long XYZ table with a range of motion of 0.2 m by 0.2 m by 6 m. (By convention, the direction of the beam was labeled as the OLYMPUS Z-axis, the Y-axis pointed up, and the X-axis pointed toward the left sector, forming a right-handed coordinate system.) This long table was supported by two large XY tables that augmented the X and Y ranges each by 1 m. The range of motion was further extended in X by substituting rods of different lengths and in Y by adding a vertical extension piece. The apparatus was used to measure the field over a grid of points on the left sector, before being transported and reassembled for a similar measurement of points on the right sector. The grid extended from -0.5 m to 3.5 m in Z. In X and Y, the grid was limited to the triangular space between the coils, but extended to ± 2.7 m on either side of the beamline. The grid points were spaced 0.05 m apart in the region within 1 m of the beamline, and 0.10 m apart in the outer region, where the field changed less rapidly. In total, approximately 35,000 positions were measured, including the downstream beamline region, which was measured redundantly from the left and the right.

After the initial setup of the apparatus, the precise position of the XYZ tables was measured with a laser tracking station over the course of a typical scan in Z. This showed that the Hall probe position varied in X and Y as a function of Z during a scan, but that the shape was quite reproducible. To correct for this variation, the start and end points of each scan were measured using a theodolite and a total station. This data then allowed the position of the Hall probe to be determined for each measurement.

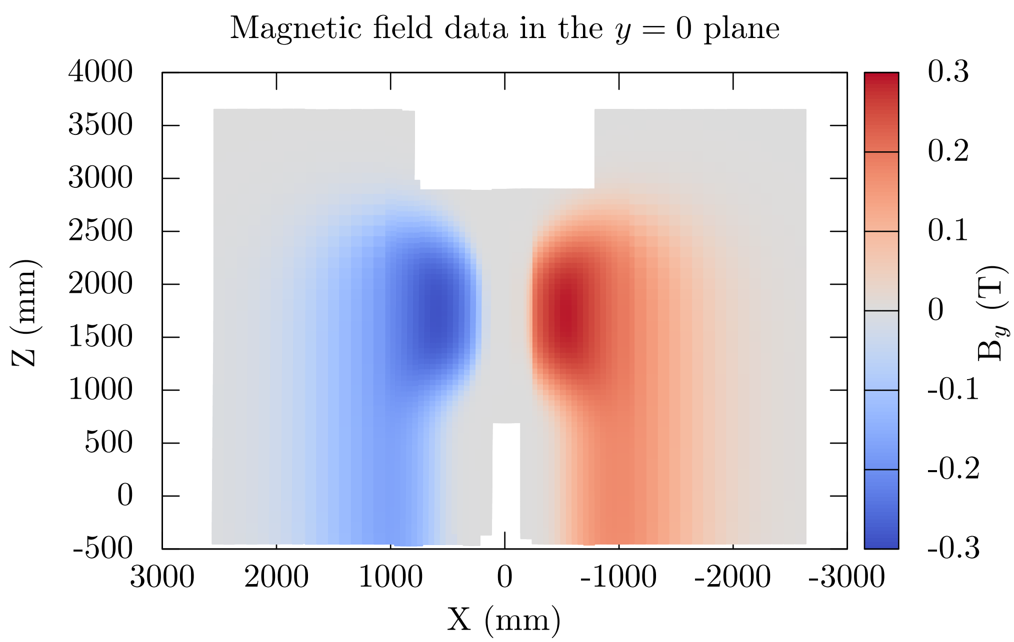

Fig. 11: The data from the magnetic field measurements in horizontal plane as viewed from above

After correcting the Hall probe positions, a fit was performed to the magnetic field data. The fit was based on a model of the coil geometry with a Biot-Savart calculation of the magnetic field. The fit allowed the coil positions to vary slightly to best match the measurements. This model was then used to extrapolate the field over the entire volume around the OLYMPUS detector for use in track reconstruction and in the OLYMPUS Monte Carlo simulation.

4.2. Drift Chambers

The drift chambers used for the OLYMPUS experiment came from the BLAST experiment at MIT-Bates and have been described in great detail elsewhere (14), so the following description will be brief while mentioning new and updated features.

The drift chambers were used to measure the momenta, charges, scattering angles, and vertices of out-going charged particles. This was achieved by tracking those particles in three dimensions through the drift chambers, which were positioned within the toroidal magnetic field. Reconstructing a particle's trajectory backwards to the scattering vertex allowed the scattering angles and vertex position to be determined. Measuring the curvature of a trajectory yielded the particle's momentum, while the direction of curvature indicated the sign of particle's charge. The drift chambers had a large angular acceptance and nominally subtended a range of 20°–80° in polar angle and a ±15° range in azimuth. The chambers were oriented to be normal to a polar angle of 73.54°. Because of these choices, the chambers were trapezoidal in shape (see Fig. 12).

The drift chambers were arranged in two sectors that were positioned on either side of the target, in the horizontal plane. Each sector contained three drift chambers (inner, middle, and outer) joined together by two interconnecting sections to form a single gas volume. Thus, only one entrance and one exit window were needed, reducing multiple scattering and energy loss. A cross sectional view of the top plate of one of the assembled gas volumes is shown in Fig. 13. The drift chambers combined had approximately 10,000 wires, which were used to create the drift field. Of these, 954 were sense wires, which read out the signals from ionization caused by a charged particle track.

Each chamber consisted of two super-layers (or rows) of drift cells, with 20 mm separation between the super-layers. The drift cells were formed by wires in a "jet style" configuration. Fig. 14 shows a cross-sectional view of a portion of one chamber with the two super-layers of drift cells. It also shows characteristic "jet-style" lines of electron drift in a magnetic field. Each drift cell was 78×40 mm^2 and had 3 sense wires staggered ±0.5 mm from the center line of each cell to help resolve the left/right ambiguity in determining position from the drift time. The wires in one super-layer were strung with a 10° stereo angle relative to wires of the other so that each chamber could localize a trajectory in three dimensions.

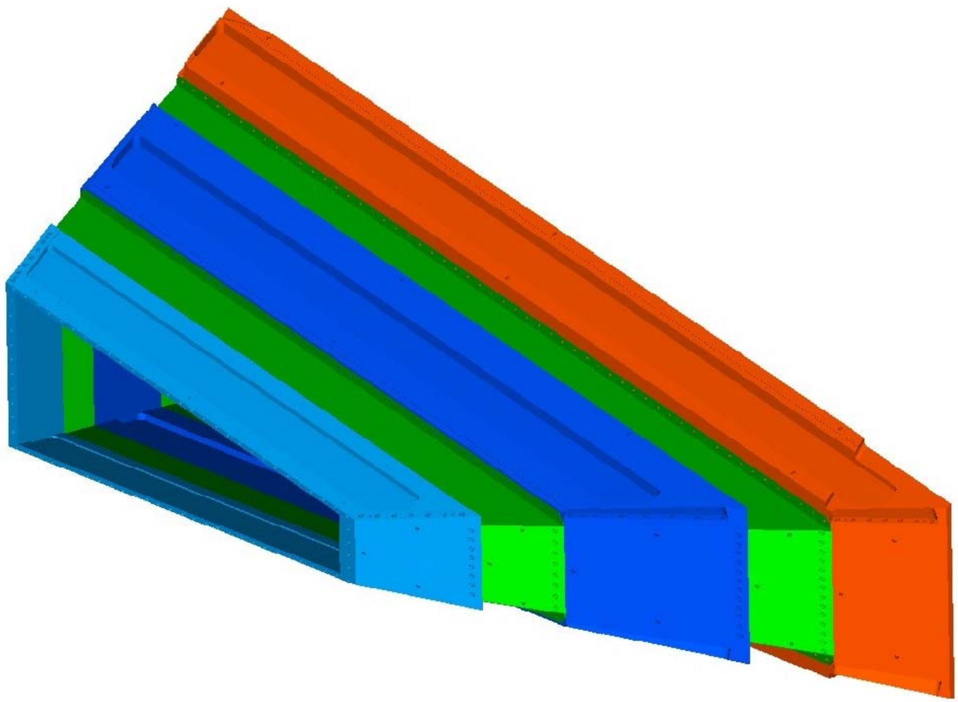

Fig. 12: Isometric view of all three drift chambers assembled into a single gas volume.

Because transporting the chambers in a way that would protect the wires from breaking was infeasible, the chambers were unstrung before being shipped from MIT-Bates to DESY. The chambers were then completely rewired in a clean room at DESY over a period of about three months during the summer of 2010. In addition to new wires, improvements were made to the front-end electronics, building on experience gained from BLAST.

For the experiment, an argon:carbon dioxide:ethanol gas mixture ($87.4 : 9.7 : 2.9$) was chosen for the drift chambers. The ethanol was added by bubbling the argon:carbon dioxide gas mixture through a volume of liquid ethanol kept at $\sim 5°$C. The chambers were maintained at a pressure of approximately 1 inch of water above atmospheric pressure with a flow rate of around 5 L/min.

Signals in the sense wires were processed with front-end electronics housed in the recesses of the interconnecting sections before being sent to TDC modules in the electronics hut. The signals were first decoupled from the high-

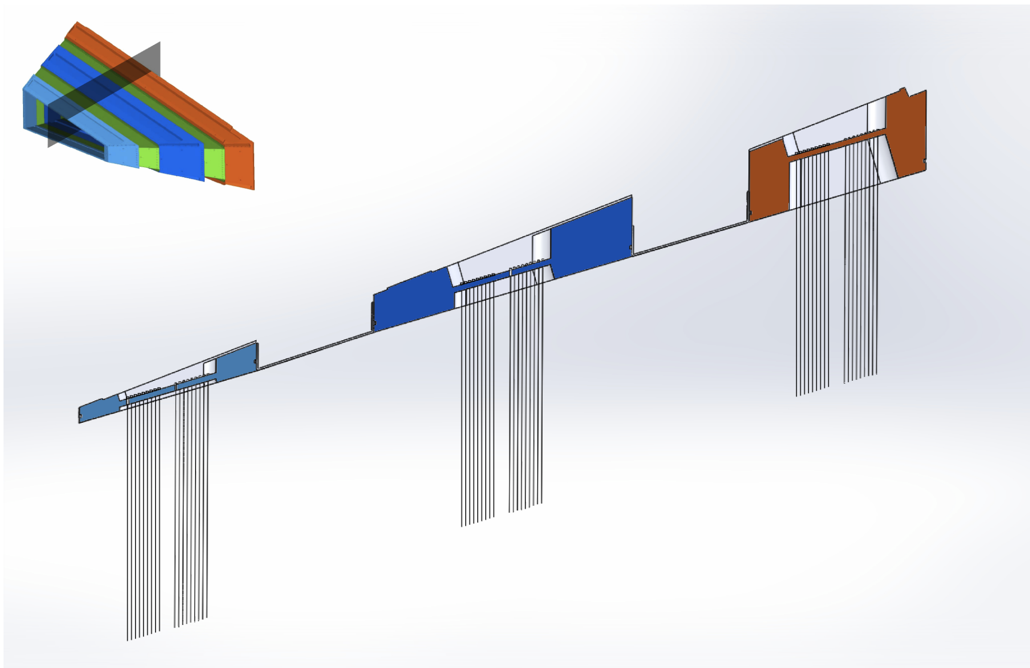

Fig. 13: Cross sectional view of the top plates of the three drift chambers and the two interconnecting sections when assembled into a single gas volume. The recesses between the top plates of the individual chambers housed front-end electronics and cables.

voltage on new, custom-designed, high-voltage distribution boards. The signals next passed to Nanometrics Systems[5] N-277L amplifier/discriminators. Then the signals were passed by Ethernet cable to the electronics hut, to LeCroy[6] 1877 Multihit TDC modules, operated in common-stop mode, with the stop signal being provided by a delayed trigger signal. The digitized signals were read out by the data acquisition system. An example TDC spectrum for a single wire is shown in Fig. 15.

[5]Nanometric Systems, Berwyn, IL, USA

[6]Teledyne Lecroy, Chestnut Ridge, NY, USA

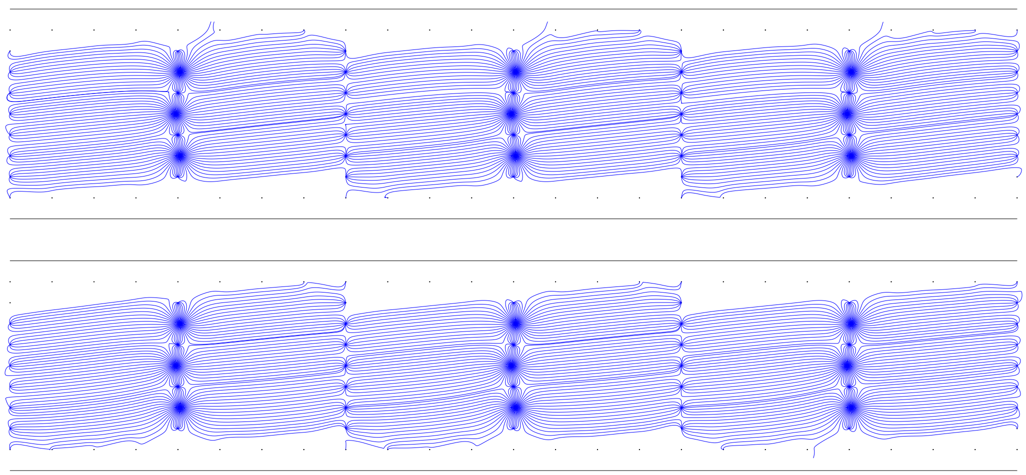

Fig. 14: Portion of a chamber showing the two super-layers of drift cells formed by wires. Lines of electron drift in the drift cells assuming a typical magnetic field around 3.0 kG are also shown.

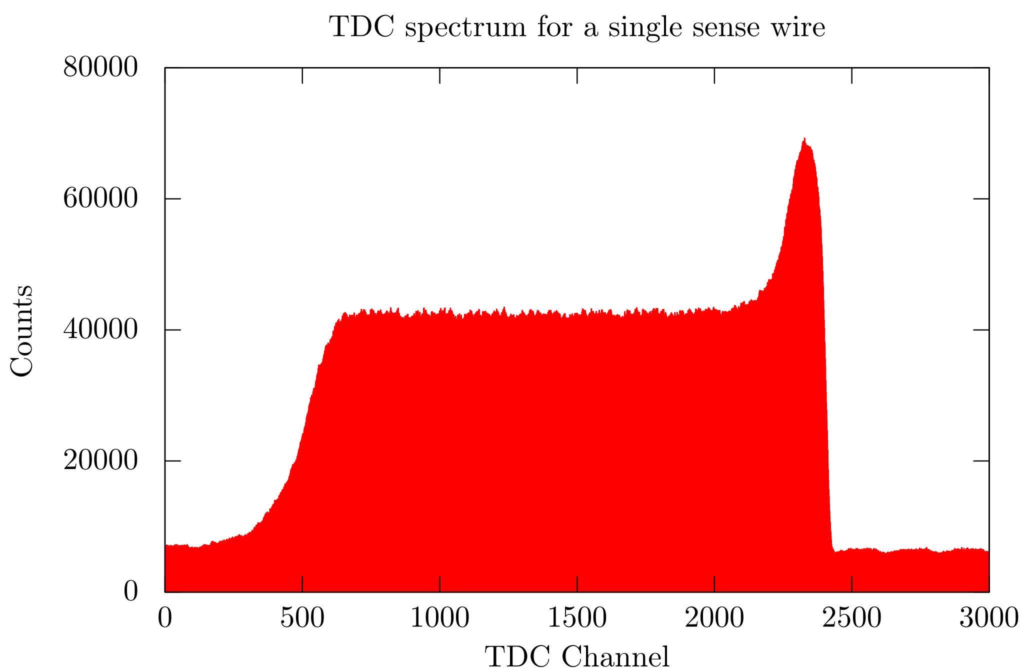

Fig. 15: A typical TDC spectrum for a single wire has a "church shape," which is characteristic of jet-style drift chambers in common stop mode.

4.3. Time of Flight Detectors

The time-of-flight (ToF) detector was adapted from system used for the BLAST Experiment (14). Each sector had 18 vertical scintillator bars with photo-multiplier tubes readout at both ends, as shown in Fig. 16. The forward four bars on each side were 119.4 cm high, 15.2 cm wide, and 2.54 cm thick. The remaining 14 bars were 180.0 cm high, 26.2 cm wide, and 2.54 cm thick.

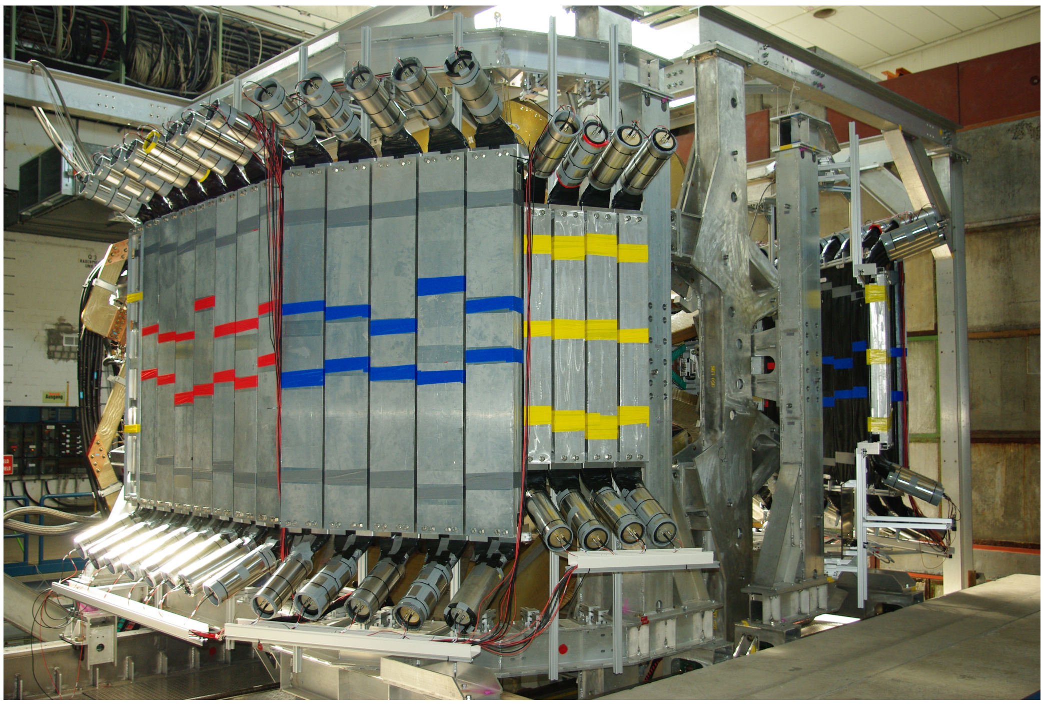

Fig. 16: ToF detector mounted in sub-detector support during assembly.

The ToF detector provided the timing signal used to trigger the readout and data acquisition system for the majority of detector components, particularly provided the common stop signal for the drift chamber TDCs. The ToF PMTs were read-out to both TDCs and ADCs. The integrated ADC signal from a given bar provided an estimate of the energy deposity in the bar while the relative time difference between the top and bottom tube signals from a bar provided a rough measurement of the hit position.

The active volume of the ToF bars consisted of Bicron[7] BC-408 plastic scintillator, chosen for its fast response time (0.9 ns rise time) and long attenuation length (210 cm). At the ends of each bar, the active volumes were connected via Lucite light guides to 3-inch diameter Electron Tubes[8] model 9822B02 photomultiplier tubes equipped with Electron Tubes EBA-01 bases. The PMT signals had a characteristic amplitude of ~ 0.8 V with a rise time ~ 8 ns. The light guides were bent away from the interaction region so as to orient the PMTs roughly perpendicular to the toroidal magnetic field. Additionally, each PMT was encased with μ-metal shielding. Each PMT base utilized actively- stabilized voltage dividers to avoid variation of signal timing with gain.

To monitor the timing and amplitude of the ToF scintillator signals, an LED flasher system was designed and installed. The main component was an LED driver powering a KingBright 7104 LED with wavelength 465 nm and luminous intensity > 3000 mCd. The light from the LED was divided into 36 optical fibers (TCU-1000W) which ran to the center of each scintillator bar. A separate fiber was connected to a fast PIN photodiode to monitor the LED amplitude.

[7] Bicron, Solon, OH, USA
[8] Electron Tubes Ltd, Ruislip, Middlesex, England

5. Luminosity Monitors

In order to measure the ratio of differential cross sections for positron-proton and electron-proton elastic scattering it was essential to measure the luminosity for each run very precisely. In OLYMPUS there were three methods to track the luminosity:

- The slow control system monitored the beam current and gas flow to the target. Knowing the temperature of the target cell and its geometry a rough calculation could determine the target density. The product of target density and beam current could be integrated over a run to give a first estimate of the luminosity.

- The 12° luminosity monitors consisting of telescopes of 3 triple GEM detectors interleaved with 3 MWPCs and triggered by plastic scintillators could measure leptons scattered over a small angular range around 12° in coincidence with proton in the wire chambers. At small angles the two-photon contribution is expected to be small so this rate gives a measure of the luminosity.

- Finally a high precision measurement using symmetric Møller or Bhabha scattering was achieved using a $PbFl_2$ calorimeter at 1.29°.

Details on the last two luminosity monitoring system are provided in the next sections.

5.1. 12° *GEM Detectors*

Six planar triple-GEM detectors with 2D strip readout were built at Hampton University and installed as part of the 12° luminosity monitor together with the MWPCs(Sec. 5.2).

The GEM detectors were designed at the MIT Bates Research and Development Center. Six gem chambers were installed, three on either side of the experiment in telescopes aligned on 12°. Interleaved with the GEM chambers are the 12° MWPCs which are mounted on an integrated support structure with the GEM chambers.

There were several considerations which drove the design of the GEM chambers. A low mass detector was desired with an active area of 10 × 10 cm. The MWPC detectors were already designed, so the GEM chamber design was required to fit in the spaces between these detectors. Finally, the collaboration took advantage of front end electronics and readout already designed and built by INFN in Rome, so the detector would need to be made to fit these cards. MITs experience designing and constructing a large area GEM detector for the FGT Upgrade to STAR at RHIC also provided design insight to make the detector easy to construct and robust.

Each individual GEM chamber was constructed of a stack of frames and foils glued together (see Fig. 17). Each stack has a readout board with three gem foils and a cathode above the active area. Two pressure volume foils form the outermost layers of the stack. All of the electrical and gas connections are accessible on the edges of the stack, or in special cut outs for the high voltage connections.

The GEM foils were manufactured by TechEtch in Plymouth MA. Each GEM foil has a 10 × 10 cm active area. The GEM foil consists of 2 mil copper clad Kapton foils perforated with 70 μm holes at a 140 μm pitch over the entire area of the detector. The GEM foils are glued to a G10 frame, manufactured by Circuit Connect in Nashua, NH. The GEM foils were placed on a stretching fixture to ensure their flatness. Then epoxy is applied to the frame and the two are glued together. Special glue grooves in the frame prevent excess glue from seeping into the active area of the foil. The foils are all tested individually before they are glued together in a stack. A clean environment is critical when performing these steps in order to ensure dust and other contaminants do not destroy the foils.

The GEM foils represent a very large percentage of the cost for the detectors. Much of this cost is the production of the tooling specific to each

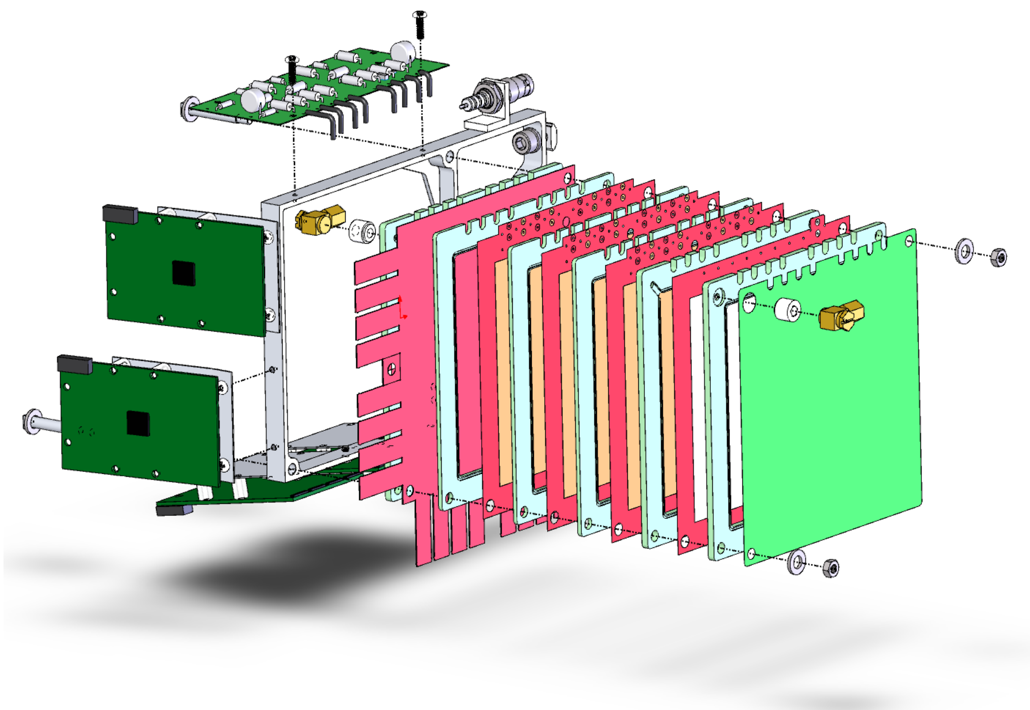

Fig. 17: Exploded view of the GEM detectors.

different type of foil. Because of this, a single foil was designed to be used in all three layers. Similarly, the frame is the same for all three layers. Cutouts in the frame provide a means for the bias voltage to be applied to each foil.

A special cathode foil is made of a piece of 2 mil copper clad Kapton with no holes in it. It provides a uniform electric field for the primary ionization area. This foil is similarly stretched and glued to a frame which is slightly thicker than the regular GEM frames. There is a pressure volume foil on top of the cathode foil and below the readout foil. This prevents the gas pressure inside the detector from bowing the readout foil or the cathode foil. The pressure volume foils were made of aluminized Mylar to provide some electrical shielding for the detector.

The readout foil was manufactured by TechEtch in Plymouth, MA. The foil consists of a 2 mil copper clad Kapton foil. On the charge collection side of the foil there are pads and lines (see Fig. 18). The lines aligned vertically

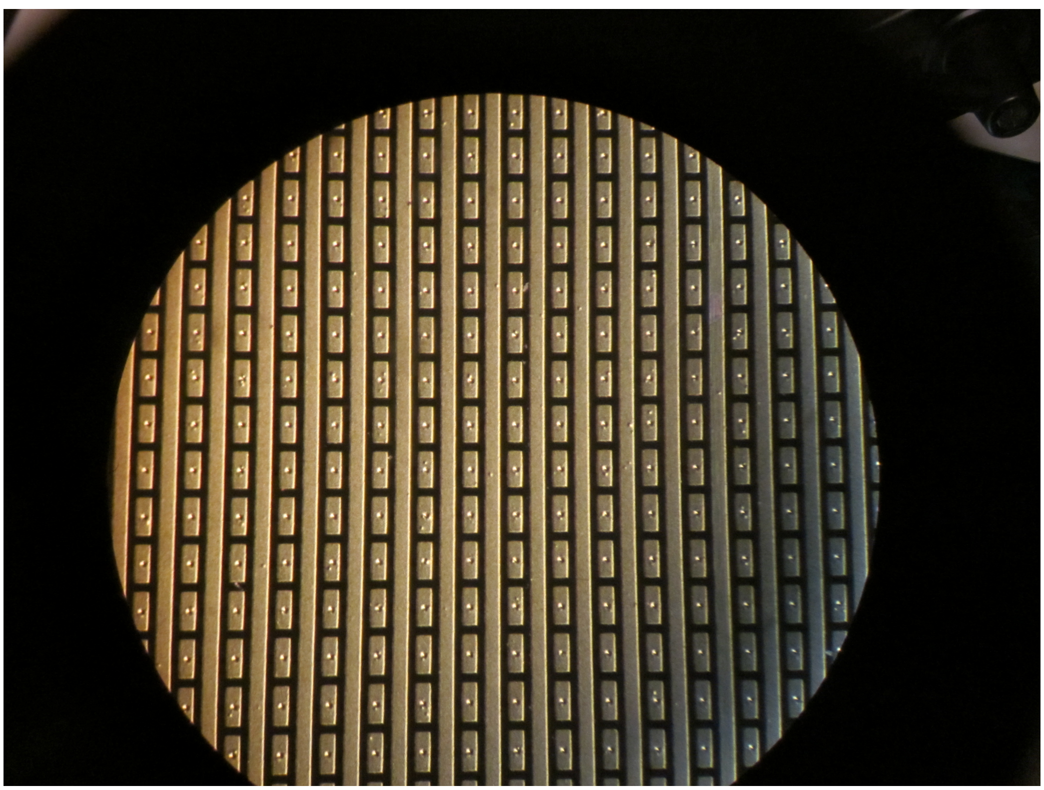

Fig. 18: View of the GEM readout foil.

and read out the horizontal coordinate. The pads each have a via and are connected on the backside of the foil with a trace which connects the pads to form rows. In this way the pads read out the vertical coordinate. The lines measure 124 μm wide, at a 400 μm pitch. The pads measure 124×323 μm, also at a 400 μm pitch. The spacing between the pads and the lines is 76 μm. The spacing between pads is 70 μm.

The signals from the lines were routed to one side of the foil, and the signals from the pads were routed to another side of the foil. These lines terminated on sixteen small arrays of pads designed to fit a flexible circuit connector which was mounted on the front end electronics card. Each card had four connectors, and there were two cards per coordinate for a total of four cards per GEM detector. Each GEM detector has 500 channels (250 per coordinate). This is a total of 3000 for both telescopes. The readout card uses the APV25-S1 analog pipeline chip. Each of the front end electronics cards designed by INFI had one these chips, along with the necessary infrastructure to read these signals out to the DAQ system. Each chip has 128 channels, each of which has a 192 cell analog pipeline which samples the input channels at 40 MHz. Data is read out of the pipeline after a trigger event. All 128 channels are multiplexed onto a single data line which then runs to the DAQ system. All of the electronics are passively air cooled.

All of the components were tested individually before they were assembled into a detector. Frames with foils mounted on them were stacked and glued together. There is a 2 mm space between each GEM foil and between the last GEM foil and the readout board. The pressure volume foils and the high voltage foils have a 3 mm space between adjacent foils. A simple resistive divider card provides the high voltage to all foils.

The finished detectors were mounted on an aluminum mounting bracket attached to the mounting rails that also hold the MWPCs. The mounting bracket had flexible supports for the high voltage card and for the front end electronics cards. These allowed the position of the cards to be adjusted during installation to avoid interferences. Both the mounting bracket and the mounting rails were adjustable. Fiducials located on the GEM chambers allowed for survey after the mounting has been adjusted. The mounting system was designed to an angular tolerance of 0.175° and a rectangular tolerance of ± 1.038 mm. Simulations show a maximum displacement of 0.672 mm which occurs on the middle chamber of the telescope. The total length of the telescope is 680 mm. The three tracking planes were located at distances of 187, 227, and 287 cm from the target, respectively, centered at

12° facing the target for perpendicular impact angle. Each telescope covered a solid angle of 1.2 msr, determined by the active area of 10×10 cm^2 and the distance of the farthest element of the telescope from the target.

An Ar:CO2 70:30 gas mixture flowed through the detector. Fig. 19 shows

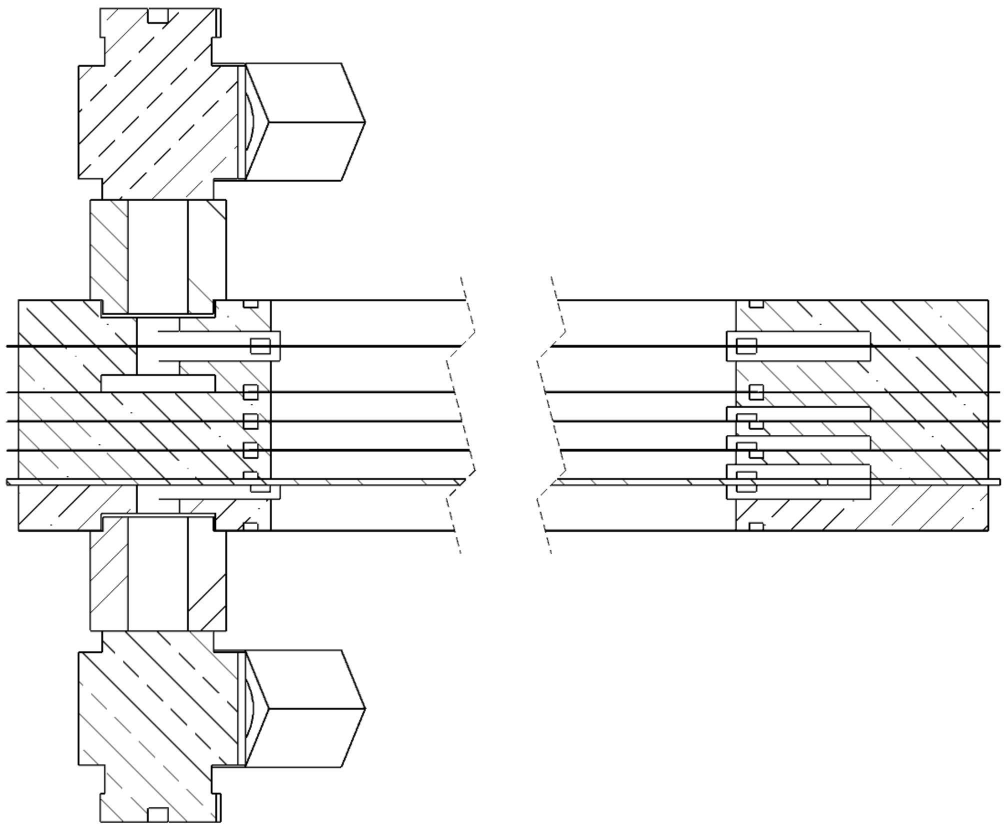

Fig. 19: Gas flow scheme for the GEM detectors

the gas flow scheme that ensures adequate gas flow across all foils. Inlet and outlet fittings are glued onto the outer pressure volume foil frames.

5.1.1. 12° *Trigger*

Each 12° telescope had two $100 \times 100 \times 5$ mm^3 scintillator tiles with SiPM readout. These were used to provide a trigger signal.

A lead glass calorimeter consisting of four lead glass bars with PMT readout was mounted behind the telescope. This detector could also be used to provide a trigger and dedicated runs were made to measure the efficiency of the scintillator trigger.

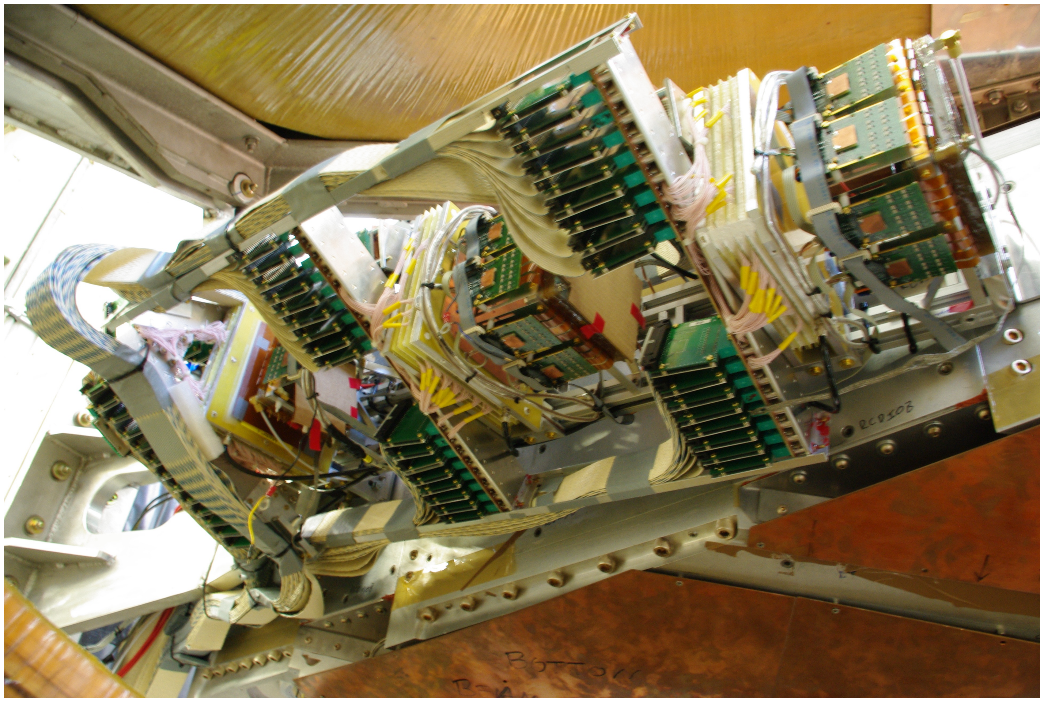

Fig. 20: Photograph of one of the 12° telescopes showing the GEM and MWPC detectors.

5.2. 12° *Multi-Wire Proportional Counters*

For the task of DORIS electron beam luminosity monitoring in OLYMPUS experiment it was proposed to use two blocks of MWPC (Multiwire Proportional Chambers). Each block of three MWPC is aligned along the axis going at the angle of 12° with respect to the interaction point at the left and right (creffig:12deg).

One MWPC module consists of three anode planes of sense wires U, X and V interleaved with the cathode wire planes. The sense wires have a 1 mm spacing and consists of 25 micron diameter gold-plated tungsten. The U and V wires are tilted by ±30° with respect to the vertical X wires. The cathode planes consist of 90 micron diameter beryllium bronze wires with 0.5 mm spacing. The general parameters for MWPC are presented in Table 1. Both anode and cathode electrode frames are made from fiberglass. These frames are sandwiched between two 10 mm thick aluminum frames.

The location of the MWPC blocks between the OLYMPUS magnet coils in vicinity of the beam pipe imposed several constrains on the detector modules design. Therefore the outer dimensions of the MWPC and positioning of

Active area	112×112 mm^2
External dimensions	$180 \times 180 \times 50$ mm^3
Anode planes	X (0°), U (+30°) and V (−30°)
Gap between anode and cathode	L=2.5 mm
Sense wire spacing	S=1 mm
Cathode wire spacing	S_{cath}=0.5 mm
Sense wire diameter	D=0.025 mm Au-plated tungsten
Cathode wire diameter	$D_{\rm cath}$= 0.090 mm beryllium bronze
U, V angle wrt X wire	±30°
MWPC material in acceptance	$\sim 0.25\%$
Working gas mixture	65%Ar+30%CO_2+5%CF_4
Gas gain at work point	$\sim 5 \times 10^4$

Table 1: Working parameters of MWPC module

the front-end CROS 3 readout electronics was simulated with GEANT3 and 3D CAD programs. This resulted in cut of frames corners from the beam pipe side on $\sim 8\times10$ mm^2. Front end electronic cards of the MWPC modules were aligned along the planes of the OLYMPUS magnet coils (Fig. 21).

As a working gas mixture MWPC use 65%Ar+30%CO_2+5%CF_4. This gas mixture was used for the magnet chambers(16) in the HERMES experiment and provided a stable operation of the detectors with good aging resistance. To evaluate high voltage working point for MWPC the gas gain dependence on applied high voltage was calculated using a GARFIELD program(17). Fig. 22 presents the calculated dependence of gas gain from the high voltage in 65%Ar+30%CO_2+5%CF_4 gas mixture. One can see that at HV=3150 V the gas gain reach about 5104. This simulation meets with results of the experimental measurements with produced in PNPI detectors. Eventually the working point at MWPC during the experiment was 3200 V.

The measuring of the MWPC operation with CROS3 electronic demonstrated a good performance of each MWPC block mounted in OLYMPUS magnet gap. Fig. 23 shows the wire map for the left (LM_L1-3(U,X,V)) and right (LM_R1-3(U,X,V)) detectors. A few channels were lost because of the contact imperfections in the cards connectors.

Track reconstruction is done using two different tracking algorithms. One method (TrackFitter) uses iterative procedure and GEANT4 tracking routine to match the track for given hit combination. Another method (KalmanFilter) uses Kalman filter algorithm for hit selection and track propagation in

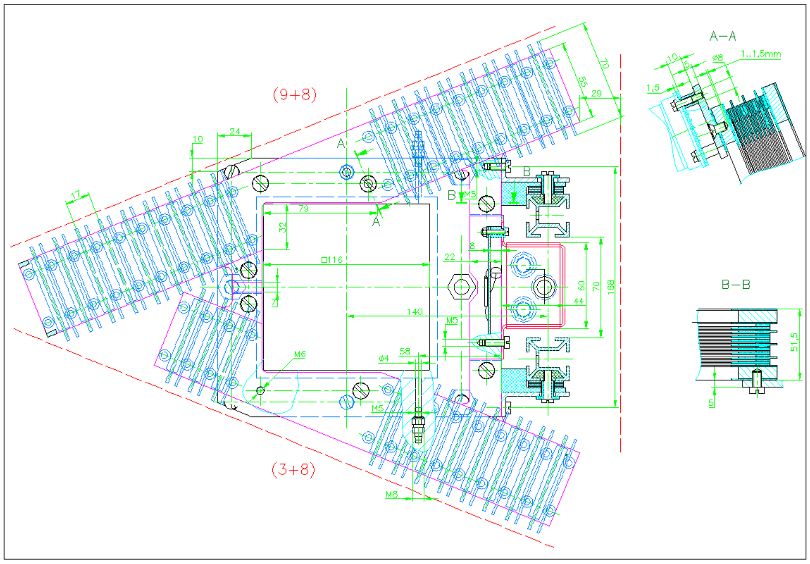

Fig. 21: Plan view of a MWPC detector assembly showing the square, active area in the center, the surrounding electronics, and the mounting fixtures.

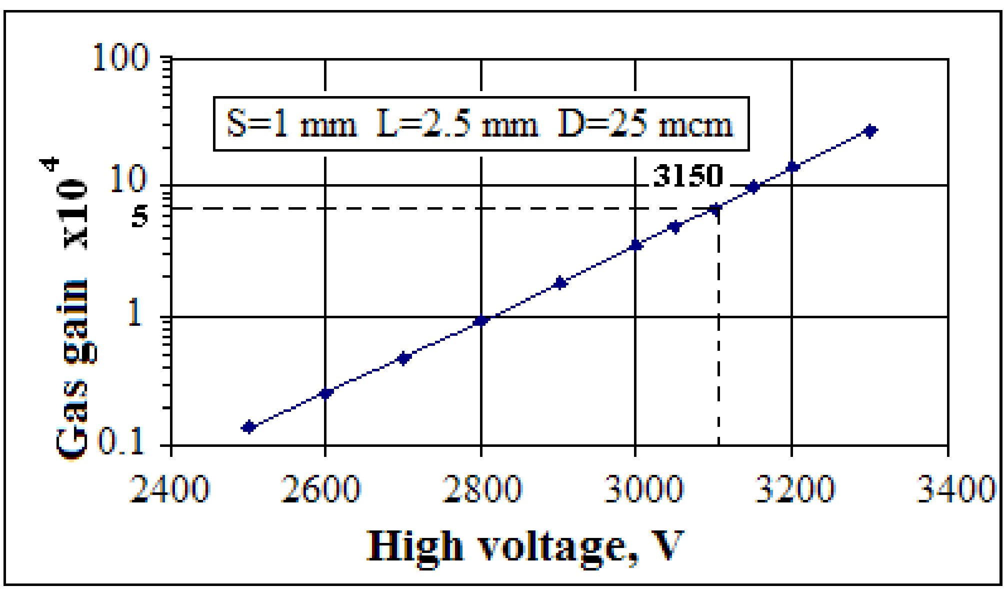

Fig. 22: Gas gain as a function of operating voltage for MWPC.

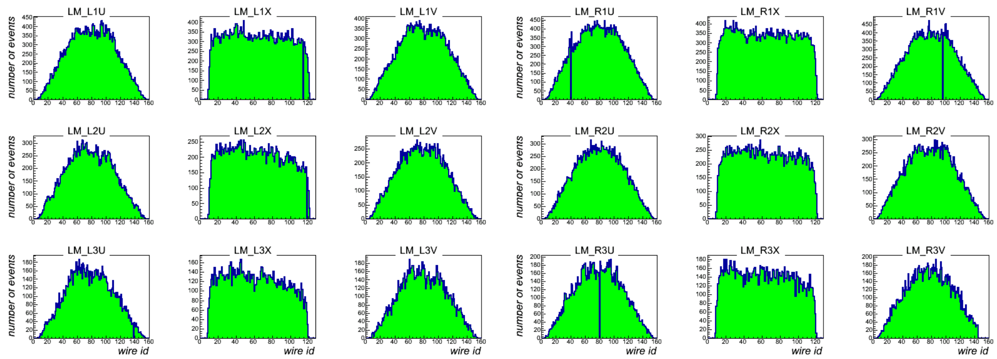

(a) Left MWPC telescope (b) Right MWPC telescope

Fig. 23: Wire hit distributions for the left and right MWPC telescopes showing the XUV planes for the three detectors.

magnetic field. Figure 5 shows charge lepton scattering angle (θ) for reconstructed tracks for various combination of the beam charge and magnet field direction. Even combination (++ or –) has a smaller average angle and correspondingly high cross section due to in-bending curvature then odd ones. Target density distribution along the beam is very well describe by primary vertices.

5.3. Symmetric Møller/Bhabha Luminosity Monitor

The symmetric Møller/Bhabha luminosity detector (SYMB) was designed to monitor the luminosity by measuring symmetric lepton scattering $e^-e^- \to e^-e^-$ (Møller) and $e^+e^- \to e^+e^-$ (Bhabha) and $e^+e^- \to \gamma\gamma$ (Annihilation). For a beam energy of 2.01 GeV symmetric scattering occurs at a polar angle of 1.298° with respect to the incident beam direction (see Fig. 24). The cross

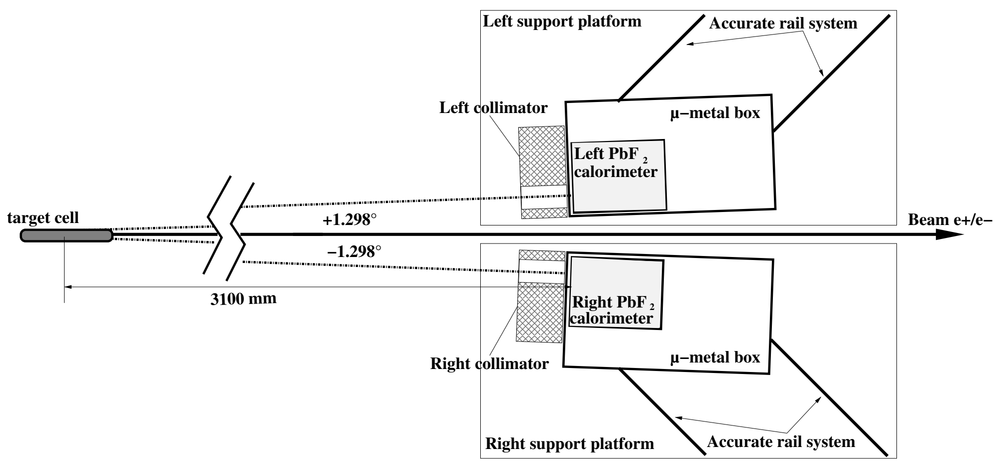

Fig. 24: Schema of the Symmetric Møller/Bhabha luminosity detector (SYMB) is shown. The collimator and the calorimeter are align at a polar angle of 1.298° with respect to the incident beam direction. The collimator is in front of the calorimeter which is inside a μ-metal boxes.

section for these processes can be precisely calculated from QED with the caveat that the annihilation reaction $e^+e^- \to \gamma\gamma$ must also be included with Bhabha scattering. By placing a pair of detectors at the symmetric angle (see Fig. 25) and measuring the rate of the Møller, Bahbha and Annihilation events by a coincidence of the left and right detector the luminosity could be determined.

The SYMB was built in Mainz. It consists of two symmetric 3×3 arrays of lead fluoride (PbF_2) crystals. The photomultipliers tubes (PMTs) were manufacture by Philips, model $XP\,29000/01$ (see Fig. 26). The dimension of the tapered crystals are about $26 \times 26 \times 160\,\text{mm}^3$. The PbF_2 has a radiation length of $X_o = 9.3\,\text{mm}$ and a Moliére radius of around 18 mm. Accordingly the 3×3 array of crystals corresponds to about 17 radiation lengths and 2.17

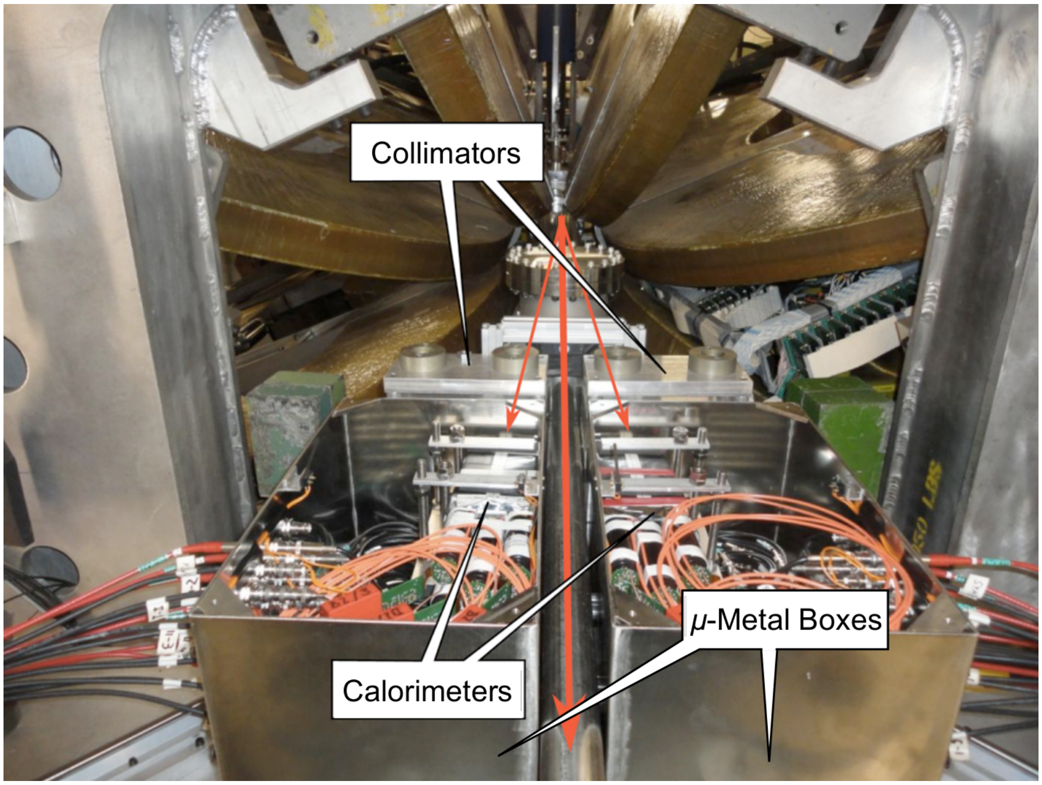

Fig. 25: The Symmetric Møller/Bhabha luminosity detector. The top of the collimator and the calorimeter is shown. The calorimeter is sitting on a support table, where an accurate rail system is located. The collimator is in front of the μ-metal boxes. The thick red line indicates the direction of the beam while the thinner red lines indicate the general path of scattered electrons and positrons entering the SYMB.

Moliére radii which is sufficient to contain $98,9\%$ of the transversal electromagnetic shower within a very compact volume. PbF_2 is a pure Cherenkov material with a very fast response and no delayed components due to scintillation light. In combinade with the PMT the signal response is 20 ns making this an extremely fast calorimeter. This enables the SYMB luminosity monitor to operate at the high rate expected at such a small angle. Each crystal was wrapped with Millipore paper to increase the reflectivity. Each detector array was placed inside a μ-metal box to shield the PMTs and the electronics from the magnetic field of the experiment toroid and the beam line magnets.

A 100 mm thick lead collimator was placed upstream of the detector arrays to shield the crystal from beam bremsstrahlung, Møller/Bhabha scat-

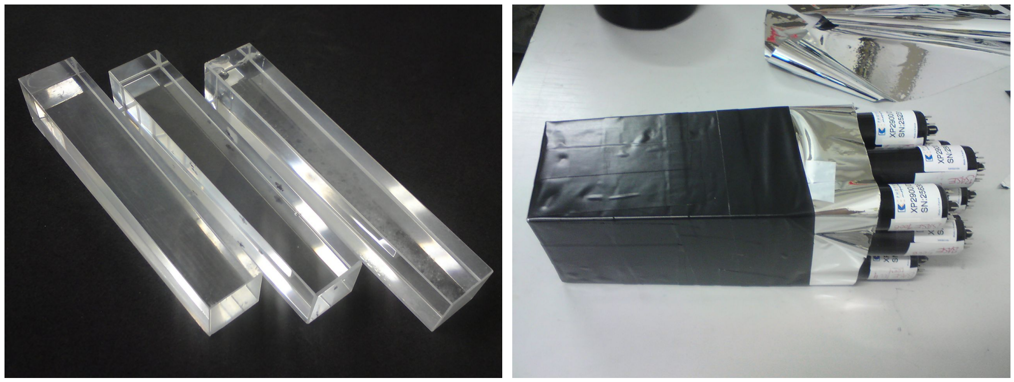

Fig. 26: Left picture show the PbF_2 crystals used in the symmetric Møller/ Bhabha luminosity monitor. Right picture show the 3×3 array of wrapped PbF_2 crystals with PMT readout.

tering at non-symmetric angles, and other background. The collimator had a removeable central plug with a precision machined hole. For the OLYMPUS experiment a circular aperture of 20.5 mm diameter was chosen. This determined the solid angle covered by each calorimeter. The location and angle of the collimator aperature was carefully surveyed before and after the experimental running periods and used in calculating the expected coincidence rates.

5.3.1. The data acquisition electronics

A modified version electronics from the *A*4-experiment at MAMI, Mainz was used for the SYMB (18). This allowed a fast analogue summation of 9 signals from left and right crystal array with subsequent digitisation and fast histogramming. The system had an overall dead time of 20 ns and allowed histogramming up to 50 MHz. The expected rate from Møller coincidence events at the design luminosity is about 9.6 kHz. The rate at DORIS is 10.4 MHz (96 ns), yiedling a probability to have one Møller coincidence events per bunch of about 0.1 %.

The readout concept is show in Fig. 27. First the 9 analog signals from each crystal of one detector array are summed. This sum was split into three signals for coincidence mode, master mode, and slave mode. At the same time the 9 analog signals are compared to each other to determine if the local maximun (LM) condition is fulfilled, i.e. the center of the shower distribution is in the center of the 3×3 cluster. If this is the case and the total deposited energy is over the threshold of a constant fraction discriminator

(CFD), a trigger signal for the histograming was generated. Because of the very high event rate, no single events are readout and analogic sum S and trigger (LM×CFD) are parallel.

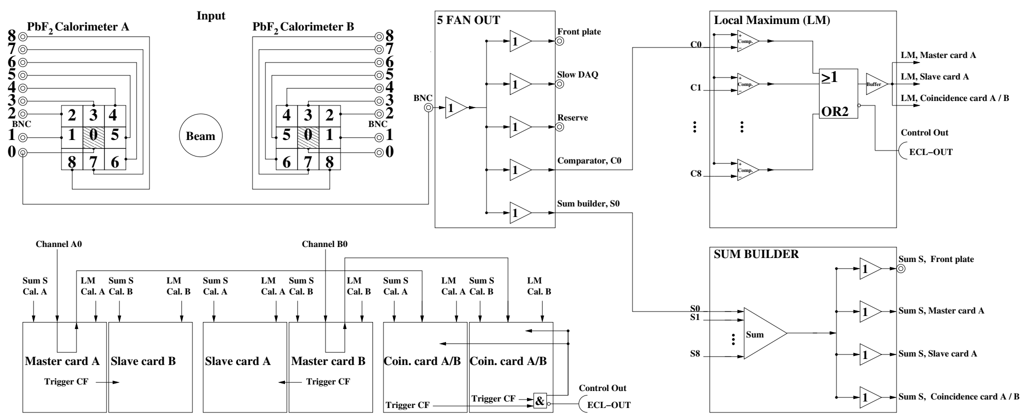

Fig. 27: The signal flow through the data acquisition electronics: input, trigger (local maximum), sum, digitization and a histogramming.

5.3.2. Event selection

Møller, Bhabha and annihilation events had the same energy deposition in both calorimeters, whereas most background events had a diferent energy deposition in the two calorimeters. Therefore, a trigger signal for histograming was produced when there was a coincident signal in both detector array exceeding the threshold (see figure 28). As a cross check a trigger signal for histograming is also produced when only one calorimeter has a signal over threshold. These three trigger signals correspond to the three histograming mode used in parallel.

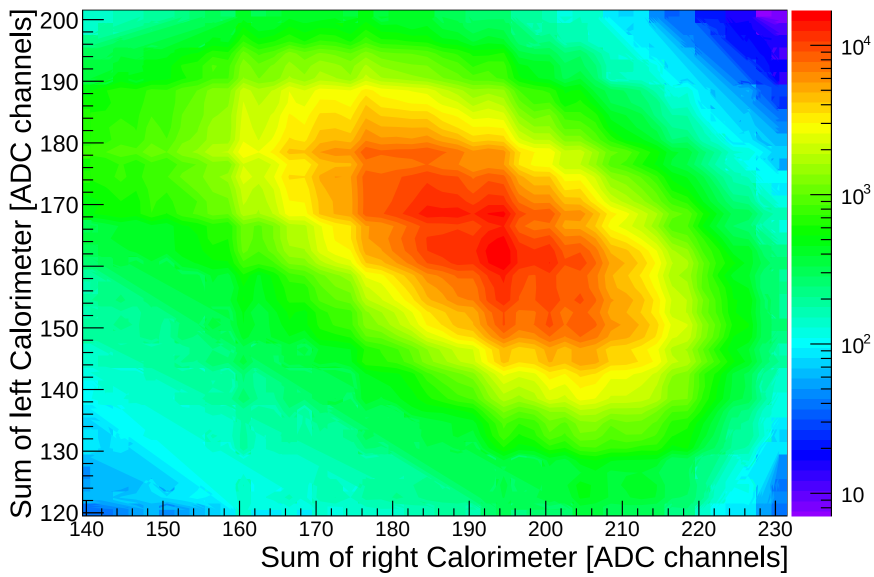

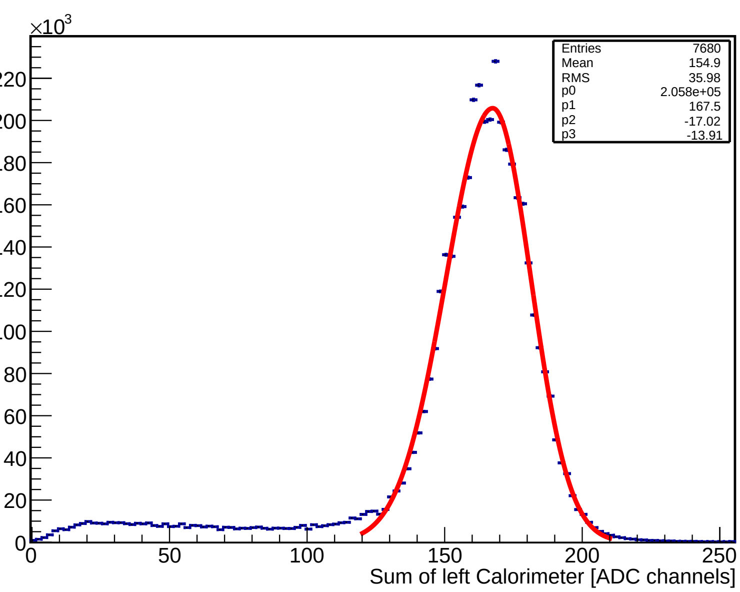

Fig. 28: Top: 2D histogram of the sum of the deposit energy on the calorimeter when the trigger signal was produced in coincidence mode. Bottom: projection of the sum of the deposite energy on the left calorimeter with differencial nonlinearity (DNL) corrected.

6. Trigger

The OLYMPUS Experiment required the development of a new trigger system that incorporated information from the reused detector components from BLAST, the new luminosity detectors, as well as information from the DORIS accelerator. This was implemented using a VME field programmable gate array (FPGA), which allowed the combination of up to 16 input signals from various systems to produce 16 parallel trigger conditions, which could be prescaled to control the rate at which different conditions were recorded.

The ToF scintillator bars and the SiPMs in the 12° luminosity monitors provided the fast trigger signals for the experiment, while the DORIS accelerator provided timing information. The primary trigger signal consisted of requiring coincidence between the top and bottom PMTs of a ToF bar in both the left and right sectors of the detector. The ToFs were grouped such that the trigger signal was produced only when the relative position of the left and right bars corresponded to the expected kinematics of an elastic $e^{\pm}p$ event. The main 12° luminosity trigger consisted of a coincidence between the two SiPMs in one sector and a ToF in the opposite sector. The DORIS bunch clock was used provided the reference time signal for the ToF and drift chamber TDCs.

In addition to the primary triggers, several signals corresponding to less strict ToF coincidences and signals from the lead glass calorimeters behind the 12° were included at higher prescale factors. Events from these triggers provided means of monitoring the efficiencies and calibration of various detector components over the course of data-taking.

During the February data run, inspection of the collected data indicated that the number of elastic $e^{\pm}p$ events in the recorded data was an unsatisfactorily small fraction of the number of triggers. To improve this for the Fall run, a second-level trigger was implemented to incorporate data from the drift chambers. The TDC signals from the drift chamber sense wires in the middle and outer chambers in each side were grouped so as to produce a second-level trigger signal only when at least one wire in each of the middle and outer chambers on each side. This signal was combined with the primary ToF trigger to form the main trigger signal for the Fall run. This scheme succeeded in reducing the false trigger rate by a factor of approximately 10, which was critical to controlling the trigger rate during high luminosity "top-up" running (see Sec. 9).

7. Data Acquisition System

The OLYMPUS data acquisition system (DAQ) utilized the framework originally developed for the Crystal Barrel Experiment at ELSA accelerator in Bonn, Germany. The implementation and hardware for the DAQ was provided by the Bonn group. The system was "synchronous" in that each detector was read-out simultaneously upon a common event signal, which ensured the event-by-event coherence of the data collected. While this approach significantly increased the complexity of the DAQ in comparison to a free-running system, reading the detector components synchronously conferred a number of advantages such as the ability to immediately identify readout errors from individual channels, definitive matching of data from different systems corresponding to the same event, and an overall increase in reliability of the system. Additionally, the system provided a graphical user interface for the control of data-taking and an integrated run database that was available via a web interface.

Synchronous operation was achieved via a master-slave hardware system. A schematic of the system is shown in Fig. 29. The system consisted of a number of 6U VME-Modules, one of which served as the *master*. The *master* module was responsible for monitoring the state of each of the *client* modules, each of which handled the signals from a set of detector elements. Each module contained a VME CPU for handling of the data readout. During data taking, each of the *client* modules signaled its state to the *master* via its "Busy+Okay" lines. The *master* generated an event trigger signal and distributed it to the clients only when all clients reported that they were functioning.

The signal sequence for the generation of a synchronous event signal by the DAQ is shown in Fig. 30. The *master* first sent an event request to the *client* modules, which responded by beginning the read-out of their detectors and reporting "busy" to the *master*. Upon completion of its readout, each *client* reported "Okay" to the *master*. Once all modules reported a successful readout, the *master* generated an event trigger signal.

Each of the VME CPUs associated with a *client* module corresponded to a specific subdetector (with some subdetectors requiring multiple CPUs) and served as a "local event builder" (LEVB) for that subdetector. The CPU associated with the *master* module served as the global event builder, in that it collected data from each of the LEVBs and checked the results for completeness before committing the data to disk. Communication be-

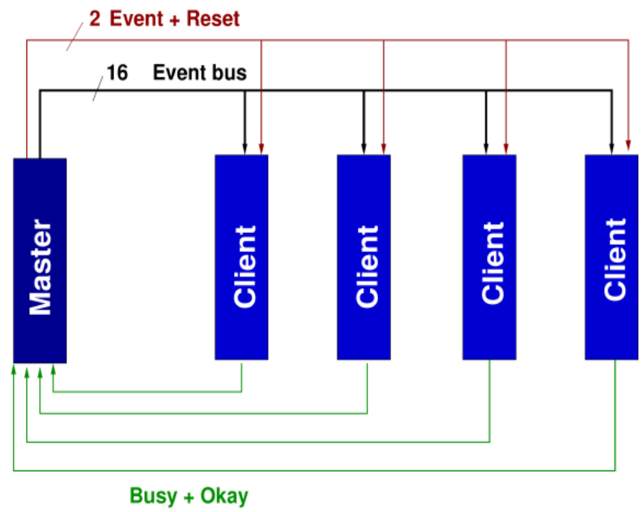

Fig. 29: Schematic of the master-slave layout of the DAQ synchronization system.

tween the global and local event builders was conducted over two dedicated 1 GBit TCP/IP networks, which allowed the separation of data transfer signals from control signals to minimize competition for bandwidth. Each of the LEVBs ran appropriate functions for interaction with the TDC, ADC, and/or scalar modules of its subdetector. The modular design of the DAQ system allowed for the construction of a synchronous readout system without excessive development time or manpower.

The global event builder featured a interchangeable output system enabling a wide variety of data formats, which provided flexibility in choosing the the optimal data format for OLYMPUS. The global event builder could achieve an output event rate of 30 kHz, which was well above the limit imposed by other elements of the detector.

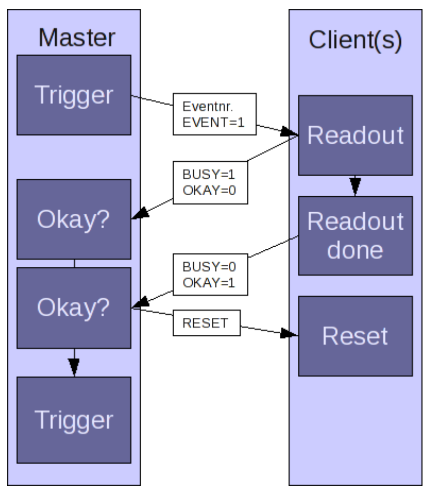

Fig. 30: Signal flow chart for the generation of an event signal in the synchronization system.

8. Slow Control

In addition to the detector electronics, trigger, and data acquisition system, successful operation of the OLYMPUS experiment required that hundreds of other components be controlled, monitored, and have their information recorded. These included the high voltages for the detectors, temperatures, pressures, flow rates and valves for the various detector gas systems as well as for the target and vacuum systems and numerous parameters concerning the beam (current, position, lifetime). Collectively, this system of control, monitoring, and recording was called the Slow Control.

The Experimental Physics and Industrial Control System, EPICS[9], was used as the back-end solution. It was deployed on three Linux machines: two VME computers with interface cards to control equipment and one server which communicated with the database and was the interface to the DORIS control system.

A PostgreSQL database stored the current status of all parameters as well as their history. The same data were also mixed into the DAQ data stream which was saved to disk.

The slow control system had a user friendly graphical user interface (GUI) using a web application, based on Flask as middleware. In contrast to more standard solutions which typically involve the deployment of custom, operating system dependent programs to any control computer, the use of web technology made it possible to have concurrent view-only and control access from any Internet-ready computer. In addition to displaying the various parameters, the simple GUI allowed to change the settings to turn detectors on or off, raise or lower high voltages, change gas flows, open or close valves, etc. The system also provided alarm features to alert the shift crew if anything was not within a predetermined range.

[9]http://www.aps.anl.gov/epics/index.php

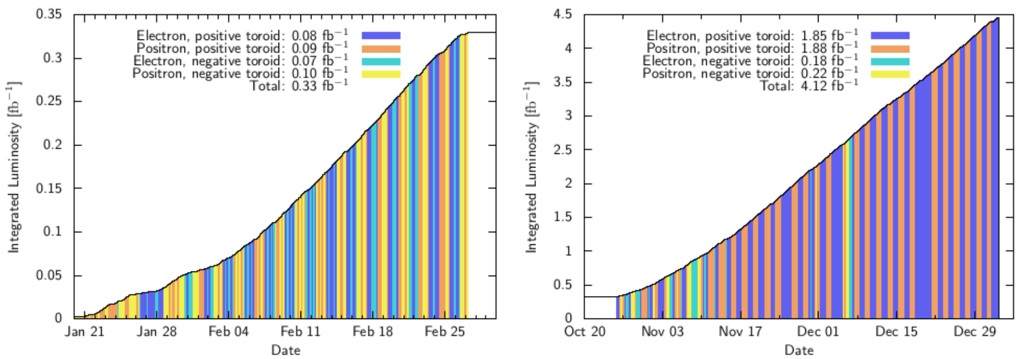

Fig. 31: The approximate integrated luminosity delivered to the OLYMPUS Experiment during the February (left) and fall (right) runs, as measured by the slow control (accurate to ∼10%).

9. Operation

During normal data-taking runs, a two-person shift crew operated the OLYMPUS detector and monitored the quality of the data using a number of plots generated in near real-time. Typically, production runs were taken 24 hours a day during the February and fall runs, alternating daily between positron and electrons beams. The integrated luminosity delivered to the experiment during the two runs is shown in Fig. 31. In total, a data set of approximately 4.5 fb^{-1} was collected over the course of both runs. As discussed in Sec. 1, density of gas in the target cell during the February run was significantly lower than the design value due to a leak in the interface between the H_2 gas feed system and the target cell. Due to this, less than 10% of the ultimate data set was collected during the February run. As is described in the following section, it was possible to run at higher average beam current during the fall run, which allowed the experiment to reach its initial integrated luminosity goals. At such higher currents, however, it was only possible to operate the experiment using a single toroid polarity (positive) due to the fact that low energy electrons were bent into the detectors in the negative polarity, resulting in an inoperable background level. Uptime during the data-taking runs was extremely high (approximately 95%), with most of the downtime accounted for by the time required (on the order of an hour) to switch the beam species daily.

9.1. Data Collection

As previously noted in Sec. 2, the experiment employed two modes of operation, differentiated by the manner in which the DORIS beam was operated. During the February run, the experiment was operated in "manual" mode in which the beam was initially filled to ∼65 mA and then data was taken as the beam decayed to ∼40 mA. At this point, the shift crew used the slow control interface (Sec. 8) to lower the high voltage of the various detectors to preset safe values. Since beam refills during the earlier running period were not as clean as during the Fall 2012 run (more instability and losses), the lowering of the voltages prevented high voltage trips and possible damage to the detectors during the refill. After lowering the voltages, the OLYMPUS shift crew informed the DORIS accelerator crew that the detector was ready for beam refill. Once the beam was restored to the normal starting current, the voltages were brought back to operational values and data-taking was restarted.

Between the February and fall runs, significant improvements were made to the DORIS beam injection process that allowed the OLYMPUS Experiment to be run in "top-up mode." In this mode, the beam was initially filled to ∼65 mA as in the manual mode, but was only allowed to decay to ∼58 mA before triggering an automatic refill. Due to the improved injection, it was not necessary to lower the high voltage of the OLYMPUS detectors during these injections. The DAQ was configured to briefly inhibit data-taking during injection pulses (see Sec. 2). This mode of running significantly increased the average instantaneous luminosity delivered to the experiment and freed the OLYMPUS shift crew to more carefully monitor the quality of the beam and incoming data.

Due to the importance of collecting data with both positrons and electrons, the beam species was switched each morning (with occasional exceptions for maintenance, balancing the amount of data collected with each species, etc.). This ensured that there were no systematic differences between e^+ and e^- runs introduced by environmental factors such as day/night cycles, reduced traffic on the DESY campus on weekends, etc. Similarly, during the February run, in which both toroid polarities were used, data-taking was segmented into four six-hour blocks each day. The pattern of toroid polarities in the four blocks each days was selected by coin toss to ensure equal running time for each polarity while avoiding systematic effects due to the time of day and week.

In addition to production runs, empty target runs (with the H_2 gas flow shut-off and the target chamber pumped down to ring vacuum levels), zero magnetic field runs, and other test runs were taken on an approximately daily basis for the purposes of monitoring backgrounds, providing data for detector calibrations, and testing proposed changes to operations. When the DORIS beam was unavailable due to problems or maintenance, the detector was left active to collect cosmic ray data. Also, cosmic ray data were collected for approximately one month following the end of OLYMPUS productions runs in January 2013. This large cosmic data set is being used for various studies of detector efficiencies and for calibration.

9.2. Data Quality Monitoring

During data-taking, the quality of the incoming data was monitored in several stages. Real-time, online monitoring of essential parameters was implemented using the ExPlORA framework originally developed by the Crystal Barrel collaboration (19). The ExPlORA program processed the raw data ZEBRA files during data collection to produce a variety of histograms and plot of quantities versus time, such as the number of drift chamber wires hit per event, ADC and TDC distributions, DAQ deadtime, and various detector rates. The OLYMPUS shift crew had access to reference plots corresponding to those shown in ExPlORA that showed data of known good quality and data representing known possible issues. This provided the shift crew with the ability to quickly identify problems with detectors as well as problems caused by poor beam quality and take action to resolve them rather than taking low-quality data.

For the fall run, a second level of data quality monitoring by the shift crew was implemented that allowed inspection of the data in a more processed format approximately 30 minutes after the conclusion of a single data run. This program automatically ran basic analysis programs on complete datasets as they became available and presented the data to the shift crew. In a similar fashion as the real-time monitoring, this program presented histograms and plots of the recent data to be compared with data of known quality, but included higher-level information such as the properties of events with good particle track candidates and basic measures of detector efficiencies.

Additionally, the long-term performance of the detector was monitored using the slow control database discussed in Sec. 8. This provided the ability to monitor the behavior of many detector parameters over the course of the entire data-taking period to identify slow drifts and sudden changes that could affect the analysis.

10. Summary

In 2012 the OLYMPUS experiment successfully collected approximately 4.4 fb^{-1} of data for electron and positron elastic scattering from hydrogen at the DORIS storage ring at DESY. The experiment used a large acceptance, left/right symmetric detector system based on a toroidal magnetic spectrometer with drift chambers for tracking, time-of-flight scintillators for triggering and relative timing, and a redundant set of luminosity monitors. A flexible trigger and data acquisition system was used to collect the data. The experiment was explicitly designed and operated to minimize systematic errors by being left/right symmetric and changing beam species daily. The initial plan to change the toroidal magnet polarity daily was not possible because of high background rates with negative polarity. Consequently 78% of the data were collected with positive magnet polarity and the balance with negative polarity.

This paper has provided a technical description of the accelerator, internal target, detector, electronics, and operation of the OLYMPUS experiment. Future papers will detail the analysis and physics results obtained.

11. Acknowledgments

The successful design, construction, and operation of the OLYMPUS Experiment would not have been possible without the research and technical support staffs of all of the institutions involved. In particular, we would like to acknowledge the DORIS accelerator group for providing the high quality electron and positron beams delivered to the experiment. We also gratefully acknowledge the DESY MEA and MKK groups for providing the necessary infrastructure and support during the assembly, commissioning, operation, and disassembly of the experiment. The research and engineering group from MIT-Bates was invaluable in all phases of the experiment, from disassembling BLAST and shipping compoents to DESY and overcoming numerous unanticipated problems during the installation of the experiment, particularly with the target and vacuum systems.

We would like to thank E. Steffens for numerous suggestions and helpful discussions during the initial development of the experiment.

Finally, we gratefully acknowledge the DESY directorate, particularly Prof. Heuer and Prof. Mnich, and the DESY Physics Review Committee for their support, advice, and encouragement from the start of the proposal.

This work was supported by the US Department of Energy and the Ministry of Education and Science of the Russian Federation.

Appendix A. Kinematics

Some plots of kinematics relevant to the OLYMPUS experiment and elastic lepton-proton scattering at a beam energy of 2.01 GeV are given below. The straight lines indicate the nominal angular coverage of the wire chambers, 20°–80°, and the centerline of the 12° detector telescopes.

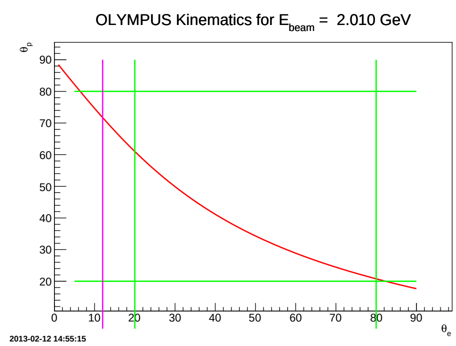

(a) Proton versus lepton scattering angle.

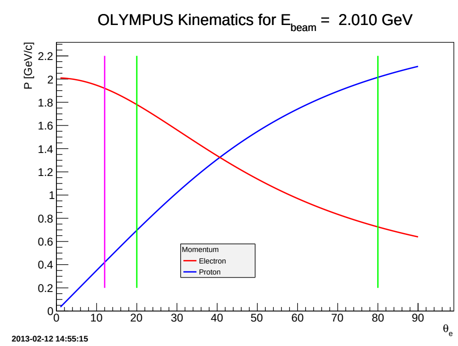

(b) Electron and proton momenta.

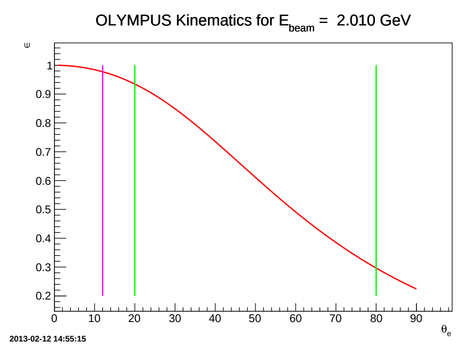

(c) Epsilon

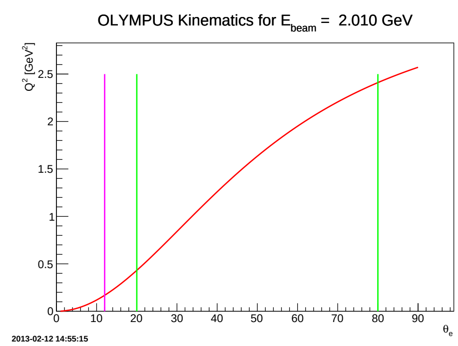

(d) Q^2

Fig. A.32

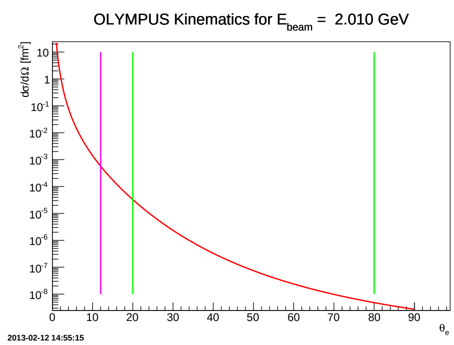

(e) Elastic *ep* cross section assuming dipole form factors.

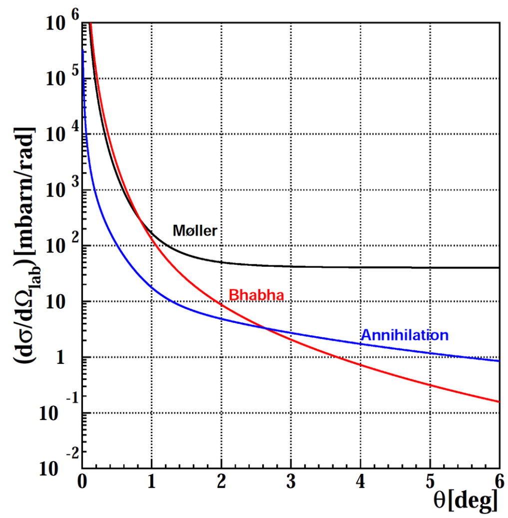

(f) Symmetric Møller, Bhabha, and annihilation cross sections.

Fig. A.32

References

[1] A. J. R. Puckett, others, Recoil Polarization Measurements of the Proton Electromagnetic Form Factor Ratio to $Q^2 = 8.5$ GeV^2, Phys.Rev.Lett. 104 (2010) 242301.

[2] M. Paolone, S. P. Malace, S. Strauch, I. Albayrak, J. Arrington, others, Polarization Transfer in the ^{4}He$(\vec{e}, e'\vec{p})^3$H Reaction at Q^2= 0.8 and 1.3 (GeV/c)^2, Phys.Rev.Lett. 105 (2010) 072001.

[3] B. Hu, others, Polarization transfer in the ^{2}H$(\vec{e}, e'\vec{p})n$ reaction up to Q^2 = 1.61 (GeV/c)^2, Phys.Rev. C73 (2006) 064004.

[4] M. K. Jones, others, G_{E_p}/G_{M_p} Ratio by Polarization Transfer in $\vec{e}p \rightarrow e\vec{p}$, Phys.Rev.Lett. 84 (2000) 1398–1402.

[5] G. MacLachlan, others, The ratio of proton electromagnetic form factors via recoil polarimetry at $Q^2 = 1.13$ (GeV/c)^2, Nucl.Phys. A764 (2006) 261–273.

[6] V. Punjabi, others, Proton elastic form factor ratios to $Q^2 = 3.5$ GeV^2 by polarization transfer, Phys.Rev. C71 (2005) 055202.

[7] S. Strauch, others, Polarization Transfer in the ^{4}He$(\vec{e}, e'\vec{p})^3$H Reaction up to $Q^2 = 2.6$ (GeV/c)^2, Phys.Rev.Lett. 91 (2003) 052301.

[8] O. Gayou, others, Measurement of G_{E_p}/G_{M_p} in $\vec{e}p \rightarrow e\vec{p}$ to Q^2 = 5.6 GeV^2, Phys.Rev.Lett. 88 (2002) 092301.

[9] I. A. Qattan, others, Precision Rosenbluth measurement of the proton elastic form factors, Phys.Rev.Lett. 94 (2005) 142301.

[10] M. E. Christy, others, Measurements of electron-proton elastic cross sections for $0.4 < Q^2 < 5.5$ (GeV/c)^2, Phys.Rev. C70 (2004) 015206.

[11] L. Andivahis, others, Measurements of the electric and magnetic form factors of the proton from Q^2= 1.75 to 8.83 (GeV/c)^2, Phys.Rev. D50 (1994) 5491–5517.

[12] R. C. Walker, B. W. Filippone, J. Jourdan, R. Milner, R. McKeown, D. Potterveld, L. Andivahis, R. Arnold, D. Benton, P. Bosted,

G. deChambrier, A. Lung, S. E. Rock, Z. M. Szalata, A. Para, F. Dietrich, K. Van Bibber, J. Button-Shafer, B. Debebe, R. S. Hicks, S. Dasu, P. de Barbaro, A. Bodek, H. Harada, M. W. Krasny, K. Lang, E. M. Riordan, Measurements of the proton elastic form factors for $1 \leq Q^2 \leq 3$ $(\mathrm{GeV/c})^2$ at SLAC, Phys. Rev. D 49 (11) (1994) 5671–5689.

[13] H. Albrecht, others, Physics with ARGUS, Phys.Rept. 276 (1996) 223–405.

[14] D. Hasell, T. Akdogan, R. Alarcon, W. Bertozzi, E. Booth, others, The BLAST experiment, Nucl.Instrum.Meth. A603 (2009) 247–262.

[15] K. A. Dow, T. Botto, A. Goodhue, D. K. Hasell, D. Loughnan, others, Magnetic field measurements of the BLAST spectrometer, Nucl.Instrum.Meth. A599 (2009) 146–151.

[16] A. Andreev, S. Belostotsky, G. Gavrilov, O. Grebenyuk, E. Ivanov, others, Multiwire proportional chambers in the HERMES experiment, Nucl.Instrum.Meth. A465 (2001) 482–497.

[17] R. Veenhof, GARFIELD, recent developments, Nucl.Instrum.Meth. A419 (1998) 726–730.

[18] R. Kothe, Design and operation of fast calorimeter electronics for an experiment for the measurement of the parity violation in elastic electron scattering.

[19] D. M. Piontek, The new online monitor for the Crystal Barrel Experiment at ELSA, 24th Students' Workshop on Electromagnetic Interactions Bosen (Saar), 2006.